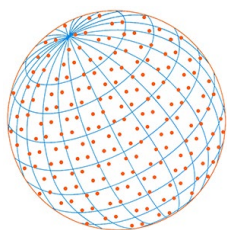


Contribution of aerosol species to the 2019 smoke episodes over the east coast of peninsular Malaysia.

NAPI, N.N.L.M., OOI, M.C.G., LATIF, M.T., JUNENG, L., NADZIR, M.S.M., CHAN, A., LI, L. and ABDULLAH, S.

2022

© The Author's institutions. This is an open access article distributed under the terms of the Creative Commons Attribution License (CC BY 4.0), which permits unrestricted use, distribution, and reproduction in any medium, provided the original author and source are cited. Supplementary materials are appended after the main text of this document.



Special Issue:

Air Pollution and its Impact in
South and Southeast Asia (III)

OPEN ACCESS 

Received: January 3, 2022

Revised: April 4, 2022

Accepted: May 12, 2022

*** Corresponding Author:**

chelgee.ooi@ukm.edu.my

Publisher:

Taiwan Association for Aerosol
Research

ISSN: 1680-8584 print

ISSN: 2071-1409 online

 **Copyright:** The Author's
institution. This is an open access
article distributed under the terms
of the [Creative Commons
Attribution License \(CC BY 4.0\)](https://creativecommons.org/licenses/by/4.0/),
which permits unrestricted use,
distribution, and reproduction in
any medium, provided the original
author and source are cited.

Contribution of Aerosol Species to the 2019 Smoke Episodes over the East Coast of Peninsular Malaysia

Nur Nazmi Liyana Mohd Napi ¹, Maggie Chel Gee Ooi^{1*}, Mohd Talib Latif ²,
Liew Juneng², Mohd Shahrul Mohd Nadzir², Andy Chan³, Li Li^{4,5},
Samsuri Abdullah⁶

¹ Insitute of Climate Change, Universiti Kebangsaan Malaysia, 43600 Bangi, Selangor, Malaysia

² Department of Earth Sciences and Environment, Faculty of Sciences and Technology, Universiti Kebangsaan Malaysia, 43600, Bangi, Selangor, Malaysia

³ Department of Civil Engineering, University of Nottingham Malaysia, 43500 Semenyih, Selangor, Malaysia

⁴ School of Environmental and Chemical Engineering, Shanghai University, 200444 Shanghai, China

⁵ Key Laboratory of Organic Compound Pollution Control Engineering (MOE), Shanghai University, 200444 Shanghai, China

⁶ Air Quality and Environment Research Group, Faculty of Ocean Engineering Technology and Informatics, University Malaysia Terengganu, 21030 Kuala Nerus, Terengganu, Malaysia

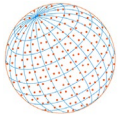
ABSTRACT

Large-scale biomass burning (BB) emits large amounts of aerosols that lead to transboundary smoke events and adversely impacts human health, whilst causing societal and environmental issues. High ambient PM_{2.5} concentration in the year 2019 based on New Malaysia Ambient Air Quality Standard (NMAAQs) was identified as high pollution episodes, HP1 and HP2 on the east coast Peninsular Malaysia (ECPM). Meanwhile, the low PM_{2.5} concentration episodes are known as LP1 and LP2. The transboundary smoke events in Indochina and Indonesia are linked to HP1 (March–April) and HP2 (August–September), respectively from backward trajectory and MERRA-2 model re-analyses weather data. The correlation analysis showed a significantly strong positive correlation (*r*) of black carbon (HP1: 0.91; HP2: 0.96), organic carbon (HP1: 0.90; HP2: 0.94), and sulphate (HP1: 0.80; HP2: 0.61) with the aerosol optical depth (AOD) levels during high pollution episodes. The synoptic weather condition and inter-monsoon in HP1 and southwest monsoon in HP2 introduce strong wind speed and favourable wind pattern that can initiate the long-range transport of high AOD and PM_{2.5} to the ECPM region. In conclusion, this study demystified the sources of BB emissions, the transport route of transboundary smoke events, their influence factors during different high pollution periods, and the links between aerosol species from local and non-local emissions with AOD levels and PM_{2.5} concentrations along the ECPM, which altogether provide crucial information on climate variability signal and can help in developing a corresponding strategy for high pollution episodes.

Keywords: Biomass burning smoke, Long-range transport, AOD, Aerosol species, East coast Peninsular Malaysia

1 INTRODUCTION

Biomass burning (BB) aerosols have a longstanding history of creating societal and environmental issues, particularly in the Maritime Continent (MC) (Tangang *et al.*, 2010; Latif *et al.*, 2018). BB aerosols released into the atmosphere contain large amounts of hazardous particulate matter and trace gases that can disrupt the Earth's energy balance by directly absorbing solar radiation and indirectly disrupting the cloud properties through aerosol-cloud interactions (Hatzianastassiou *et al.*, 2007;



Forster *et al.*, 2007; Hatzianastassiou, 2009). The continual release of black carbon (BC) and organic carbon (OC) from BB aerosols which can minimize the penetration of solar radiation reaching ground level. Consequently, it interrupts the local and regional circulation and degrades the air quality of the entire MC through transboundary smoke events (Morgan *et al.*, 2020; Tang *et al.*, 2020). BB aerosols also introduce indirect effects which are known as cloud albedo and cloud lifetime by modulating the cloud properties by increasing and decreasing the droplet concentrations and influencing the amounts of precipitation in local and regional areas (Huang *et al.*, 2019; Liu *et al.*, 2019; Jacobson, 2014). Hence, the continual uncontrolled emission of BB aerosols can cause unhealthy air quality as well as lead to the climate change problem (IPCC, 2013).

Peninsular Malaysia has unique geographical features. It is located at the middle of the MC and is surrounded by multiple countries that experience recurring large-scale BB events, hence making it susceptible to transboundary smoke events derived from BB activities. The wide South China Sea (SCS) is situated off the east coast of Peninsular Malaysia (ECPM). The coastal region, ECPM is often known to be affected by air-sea interaction processes which influence convection and the air quality of local and regional areas (He *et al.*, 2018). Hence, this study focused more on the ECPM region since it has complex weather conditions and its air quality is susceptible to the influence of large-scale BB activities that occur in Southeast Asia (Rahim *et al.*, 2021; Latif *et al.*, 2018). Similar to most coastal cities, the ECPM is influenced by synoptic and local (land-sea breeze) weather features. The main synoptic factor is the northeast monsoon (NEM) that occurs during the boreal winter. When the surface temperatures decrease in continental Asia during the winter, the outgoing cold air masses from Siberian-Mongolian highs form wet northeasterlies over the ECPM (Mohyeddin *et al.*, 2020; Ashfold *et al.*, 2017; Kok *et al.*, 2015; Ooi *et al.*, 2011). The northeasterly winds were found to introduce the BB smoke from Indochina's BB emissions to the ECPM via the SCS (Chenoli *et al.*, 2018). On the other hand, the southwest monsoon (SWM) which occurs during the boreal summer is often closely linked with severe transboundary smoke events in Indonesia. However, very limited studies have been conducted on how synoptic conditions in the ECPM region influence the long-range transport of transboundary BB smoke through the SCS, affecting air quality.

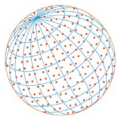
The collective analysis of backward trajectory analyses, model data, and satellite data can aid in identifying the source of emissions and dominant types of aerosols that influence the air quality during transboundary smoke events in regions of the ECPM. The aerosol product data are available from satellites, such as from the Moderate Resolution Spectroradiometer (MODIS) and Cloud-Aerosol Lidar with Orthogonal Polarization (CALIOP) while modelling data can be obtained through Modern-Era Retrospective Analysis for Research and Application (MERRA) reanalysis data. The term "aerosol optical depth" (AOD), sometimes known as "aerosol optical thickness" (AOT), was used in the model and satellite product, as it refers to how much the aerosol loading in the form of particulate matter can prevent sunlight from reaching the ground level in a column. Numerous previous studies have shown the success of those satellite and model data in simulating the relationship of aerosols with their species and the vertical profiling of aerosol species on a spatial and temporal scale (Zhang *et al.*, 2021; Rizza *et al.*, 2019; Liu *et al.*, 2018). However, in the ECPM region, MERRA and CALIOP data have rarely been used to distinguish between the dominant aerosol species from local and non-local emissions.

The main objectives of this work were to identify the high pollution periods and the sources of emissions that influence the high PM_{2.5} concentrations and AOD levels over the ECPM region. The study also attempted to identify the role of synoptic meteorological conditions that can influence long-range transport of emissions from their burning sources. The burning aerosol species in the ECPM region were also determined through the MERRA-2 reanalysis dataset during different high pollution periods. This study could provide a thorough understanding of the weather factors and aerosol species that influence the degradation of the air quality over the ECPM, thus providing important information for developing mitigation measures to improve air quality conditions.

2 METHODS

2.1 Study Period and Location

The year 2019 was selected as the study period for air quality study as it experienced two



major high pollution episodes of ambient $PM_{2.5}$ concentrations on the east coast of Malaysia (Fig. 1) and west Malaysia (Fig. S1). The high pollution periods were characterized by pollution values well above the New Malaysia Ambient Air Quality Standard (NMAAQs) limit, $35 \mu\text{g m}^{-3}$ for 24 hours (DOE, 2021). These major pollution periods coincided with BB seasons both in Southeast Asia during the boreal spring and the MC during the boreal summer (shown in Fig. 2). Hence, 2019 can serve as an exemplary case study period to determine the potential sources of $PM_{2.5}$ from burning, as well as distinguishing the difference between the $PM_{2.5}$ species from the two pollution episodes.

Malaysia recorded higher than usual average annual temperature of around 32.7°C in 2019, while the total rainfall was between 1800 mm and 3900 mm and the highest average daily wind speed was 6.6 m s^{-1} (MET, 2019). It experienced a weak El-Niño phase from early in the year until June 2019 and continued with a neutral El-Niño Southern Oscillation (ENSO) event until December 2019 (MET, 2019). The regions experienced a SWM, inter-monsoon, and NEM with occasional tropical cyclones in 2019 with distinctive typhoons in August (Lekima) and November (Nakri) across the SCS.

This study covered three states along the ECPM, namely Terengganu, Kelantan, and Pahang. The location of the ECPM increases its likelihood of receiving air pollution from various sources including long-range transport, local emissions, and natural sources. The region also faces the SCS, where the local and long-range air pollution could mix with clean marine air, making it hard to differentiate between the two. The main economic activities of these three regions include the oil and gas and petrochemical industries, and agriculture, education, tourism, and manufacturing sectors (Latif et al., 2018). One Continuous Air Quality Monitoring Station (CAQMS) was selected for each state with the highest daily $PM_{2.5}$ reading, as marked in Fig. 1: the CAQMS in SMK. Bukit Kuang (CA42T) with a latitude of 4.261° and longitude of 103.426° , SMK Tanah Merah (CA46D) with a latitude of 5.811° and longitude of 102.135° , and SK Indera Mahkota (CA40C) with a latitude of 3.818° and longitude of 103.297° , to represent Terengganu, Kelantan, and Pahang, respectively.

2.2 Data

2.2.1 Ambient $PM_{2.5}$ concentrations data

The one-year data of $PM_{2.5}$ ($\mu\text{g m}^{-3}$) from January until December of 2019 were acquired from the Department of Environment (DOE) Malaysia. The hourly $PM_{2.5}$ measurement data were measured using a particle analyzer of a Continuous Dichotomous Ambient Air Monitor 1405-DF

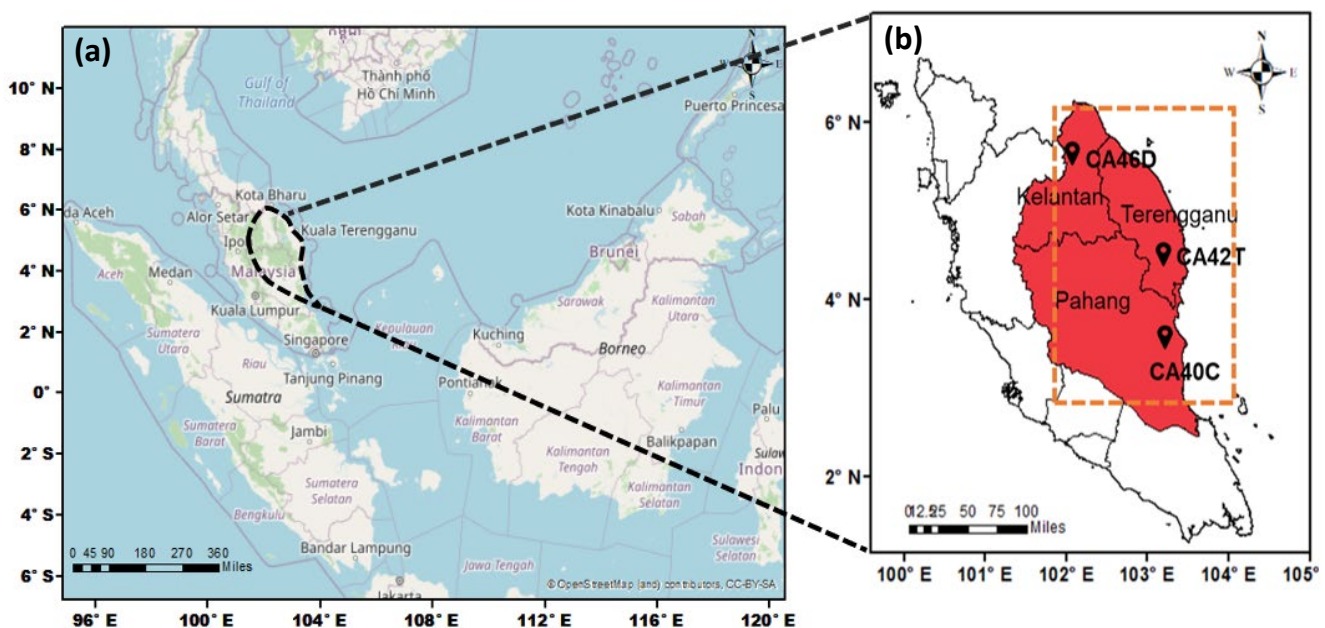
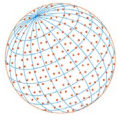


Fig. 1. The study area showing (a) the Maritime Continent, (b) the ECPM regions with the CAQMS involved in this study (shaded in red) and the MERRA-2 reanalysis data extracted for correlation analyses in the ECPM region (dotted orange rectangle).



Tapered Element Oscillating Microbalance (TEOMTM) (Azhari *et al.*, 2021). The quality of assurance and quality control of the data were conducted with a manual calibration using gas detection, to ensure the missing data resulting from technical problems were checked and verified before data was published (PSTW, 2018a, 2018b).

2.2.2 MERRA-2 reanalysis data

The AOD (550 nm) and other five aerosol species of BC, OC, sulfate (SO_4^{2-}), dust, and sea salt, as well as wind speed, wind direction, and sea level pressure (SLP) in 2019 were obtained through the through the MERRA-2 reanalysis based on the Goddard Earth Observing System Model, version 5 (GEOS-5), and together with Atmospheric Data Assimilation System (ADAS) through the open-access NASA Earth web-based data at <https://disc.gsfc.nasa.gov/> with monthly and hourly distribution data (M2IMNXGAS and M2T1NXAER) and six-hourly intervals of meteorological data (M2I6NPANA). The resolution of the data was about $0.5^\circ \times 0.65^\circ$ latitude and longitude, with 72 hybrid-eta levels from the surface to 0.01 hPa (Penna *et al.*, 2018). The Spearman bivariate analysis in the SPSS® version 25 was used to analyze the relationship of AOD with BC, OC, SO_4^{2-} , dust, and sea salt.

The hourly near-surface $\text{PM}_{2.5}$ of MERRA-2 was verified with the ground-based data model for the three stations based on the mean fractional bias (MFB), mean fraction error (MFE), and correlation coefficient (R), the equations are shown in the supplementary Fig. S2. The model agreed well with the observation data, with the MFB was slightly underestimated (around -0.02 to 0.09), MFE (up to 0.15), and R (around 0.38 to 0.72) for all three locations in the ECPM region. The ground based AOD measurements were unavailable at these stations, while standard errors of 15% were unexpected according to several previous verification studies (Yang *et al.*, 2021; Rizza *et al.*, 2019).

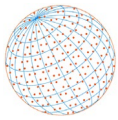
2.2.3 CALIOP data

The LIDAR level 1 version 4.1 product of CALIOP with day and night 532 nm backscatter parameters (for aerosol vertical feature masks and their subtype) were obtained from the Cloud-Aerosol Lidar and Infrared Pathfinder Satellite Observation (CALIPSO) satellite based on the period that synced with high aerosol emission detected through backward trajectory analyses of the studied ECPM regions and assessed in <https://subset.larc.nasa.gov/calipso/> (Nowottnick *et al.*, 2015; Winker *et al.*, 2010). The incorporation of the MERRA version 2 in the CALIOP validation showed an increase of the accuracy and reliability of the output. However, a small percentage of bias needed to be accounted for since the stratospheric aerosol background has a greater tendency in the tropics compared to higher atmosphere's altitudes especially in the daytime (Vaughan *et al.*, 2012).

2.3 Backward Trajectory Analysis

The Hybrid Single-Particle Lagrangian Integrated Trajectory (HYSPPLIT) model through the web-based version (<https://www.ready.noaa.gov/hypub-bin/trajtype.pl>) provided by the National Oceanic and Atmospheric Administration (NOAA) Air Resource Laboratory's (ARL) Real-Time Environmental Application and Display System (READY) (NOAA, 2021a) was used in this study to determine the sources of emissions and their transport medium to the ECPM. The meteorological dataset of Global Data Assimilation System (GDAS) data with a $1^\circ \times 1^\circ$ horizontal resolution with different horizontal and vertical resolutions over 72 hours was applied to drive the backward trajectory HYSPPLIT model in order to trace the source of higher $\text{PM}_{2.5}$ concentrations that arrived at the three selected CAQMS stations in the ECPM region (NOAA, 2021a).

Five different above-ground level (AGL) heights at 10 m (near-surface layer), between 500 m to 1500 m (boundary layer), and between 1500 m to 3000 m (free lower troposphere layer) were selected to observe the atmospheric stability and determine in which AGL level the aerosols were transported and deposited in Malaysia (Hee *et al.*, 2016). Considering some limitations of HYSPPLIT in processing the quality of complex terrains and meteorological datasets, the simulation and episodic data interpretation had to account for an estimated error of about 15–30% (NOAA, 2021b; Watt *et al.*, 2017).



3 RESULTS AND DISCUSSION

3.1 Distinct Periods of Aerosol Loading along the ECPM

In this study, the time series of ambient $PM_{2.5}$ concentrations in the year 2019 for each station along the ECPM shows a fluctuating trend as shown in Figs. 2(a–c). The hourly $PM_{2.5}$ concentrations in Terengganu, Kelantan, and Pahang were almost constantly higher than NMAAQs permissible limit throughout with two significant periods of hourly $PM_{2.5}$ concentrations in each station. The daily trends of average $PM_{2.5}$ concentrations were plotted for each station based on the CAQMS and MERRA-2 reanalysis data (Fig. S3). The AOD also showed a fluctuating trend throughout the year as shown in Fig. 2(d). Hence, four different periods were identified in this study for the maximum and minimum $PM_{2.5}$ concentrations and AOD: (i) March–April (high pollution period 1, HP1), (ii) May (low pollution period 1, LP1), (iii) August–September (high pollution period 2, HP2), and (iv) December (low pollution period 2, LP2). The minimum and maximum values of $PM_{2.5}$ concentrations and AOD are also shown in the time-series graph in Fig. 2. The average $PM_{2.5}$ concentrations at Terengganu during HP1, LP1, HP2, and LP2 were $20.75 \mu\text{g m}^{-3}$, $16.33 \mu\text{g m}^{-3}$, $39.02 \mu\text{g m}^{-3}$, and $10.92 \mu\text{g m}^{-3}$, respectively. In Kelantan, the average $PM_{2.5}$ concentrations were $28.34 \mu\text{g m}^{-3}$ (HP1), $14.57 \mu\text{g m}^{-3}$ (LP1), $26.39 \mu\text{g m}^{-3}$ (HP2), and $16.82 \mu\text{g m}^{-3}$ (LP2). Meanwhile in Pahang, average $PM_{2.5}$ concentrations of $16.38 \mu\text{g m}^{-3}$, $20.10 \mu\text{g m}^{-3}$, $42.54 \mu\text{g m}^{-3}$, and $10.04 \mu\text{g m}^{-3}$

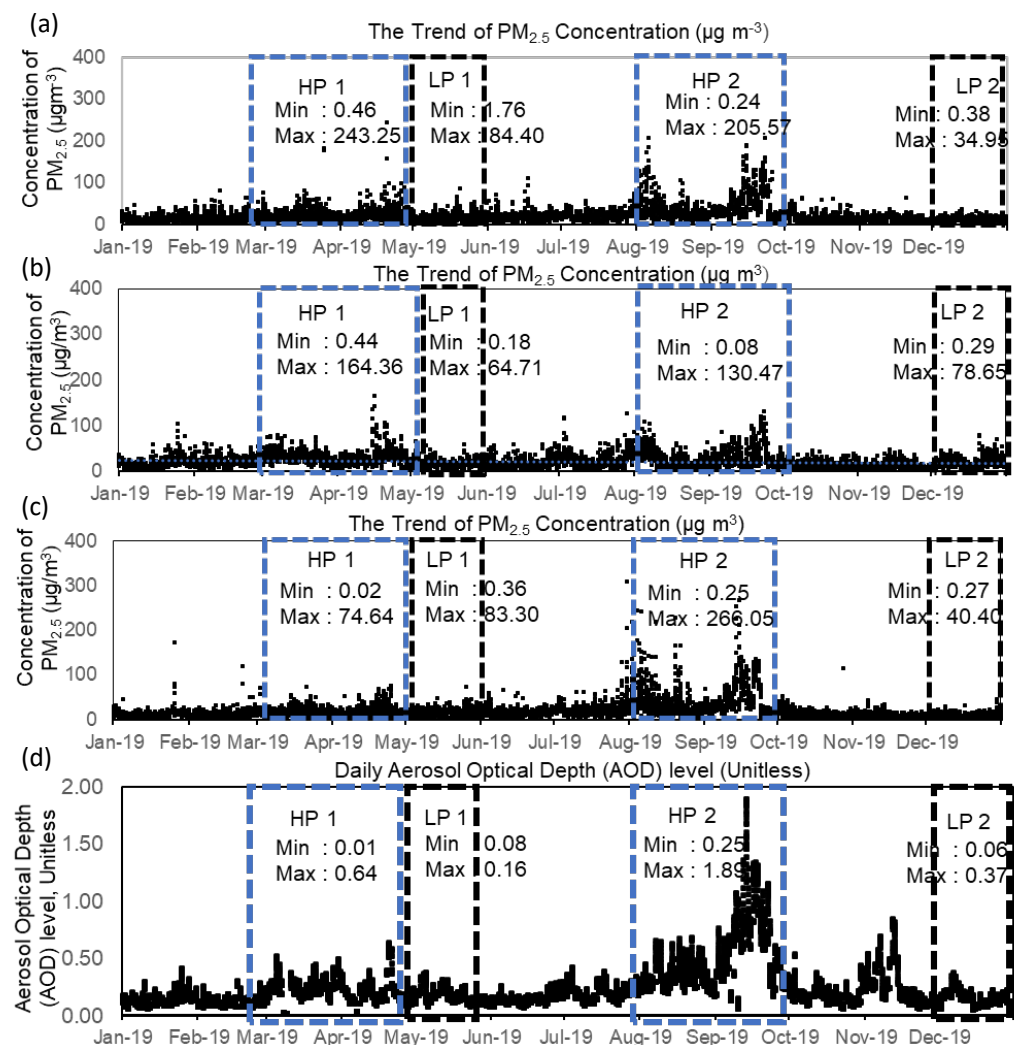
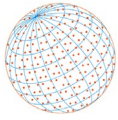


Fig. 2. Hourly $PM_{2.5}$ concentrations in (a) Terengganu, (b) Kelantan, (c) Pahang, and (d) AOD levels in the ECPM region. The periods of high pollution (HP) are marked by blue rectangles and the low pollution (LP) periods are marked by black dotted rectangles.



were recorded during HP1, LP1, LP2, and LP1, respectively. The ECPM regions had average AOD levels of about 0.22, 0.16, 0.51, and 0.16 during HP1, LP1, HP2, and LP2. This statistical analysis describes the selection criteria for high and low pollution periods at ECPM and used the DOE permissible limit of $PM_{2.5}$ concentration as benchmarks. Comparisons with Figs. 2(a–c) and 2(d) show that the $PM_{2.5}$ concentrations and AOD levels exhibited a simultaneous trend of high and low aerosol loadings during HP1, LP1, HP2, and LP2. Hence, the aerosol particles could be found in form of small and fine particulate matter (i.e., $PM_{2.5}$) in the atmosphere. The ECPM has a lower GDP (gross domestic product) than the main economic hub in west Peninsular Malaysia. Indeed, the ECPM region usually records low $PM_{2.5}$ levels compared to west Peninsular Malaysia, but the values of both increased tremendously during BB activities especially in March and September in year 2019 (Fig. 2 and Fig. S1 in the supplementary materials). This observation is also supported by findings by Samsuddin *et al.* (2018) who noted that the $PM_{2.5}$ values exhibited a two-fold increase in semi-urban and urban areas in Peninsular Malaysia during hazy days due to BB.

Figs. 3(a–l) illustrate the monthly spatial MERRA-2 AOD levels from January until December of 2019. High AOD levels were identified over two main regimes during different periods of time. From January until May, the AOD levels were higher over the Indochina region (Figs. 3(c–e)) which exerted a significant influence on the AOD levels in Malaysia from March to May when HP1 was identified. Meanwhile, from July until November, the AOD levels were higher in Malaysia and Indonesia (Figs. 3(g–k)), concurrent with the HP2 period. The AOD hotspots show that the origins and sources of the aerosols were located in Kalimantan, Sumatra, and Java.

In this study, the meteorological parameters played an important role in triggering the high AOD levels and transboundary smoke events that affected the ECPM region as shown in Fig. 4. The wind speed, wind direction, and SLP versus AOD levels at 925 hPa pressure, an ideal condition to present the influence of meteorological factors at the east coast areas (Ashfold *et al.*, 2017) were plotted to observe the long-range route of transboundary smoke to the ECPM. The transboundary smoke events in this study were defined when the level of AOD at the sources of emissions exceeded 0.5. The AOD threshold value of 0.5 in the sources of emissions was chosen as a benchmark because the levels of AOD at the origins of emissions must be higher than in the receptor regions. The minimum AOD levels during high pollution periods along the ECPM ranged

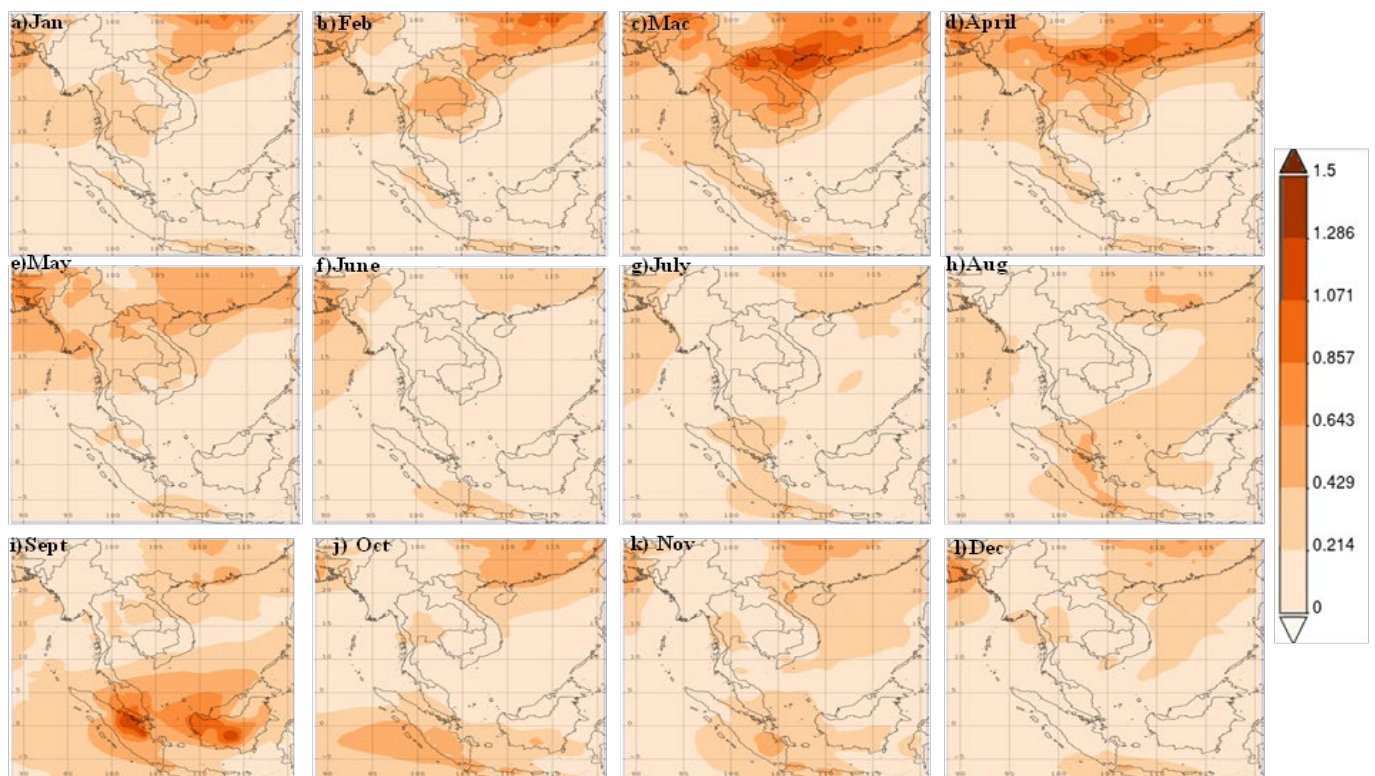


Fig. 3. Monthly AOD distributions extracted from MERRA-2 for the year 2019.

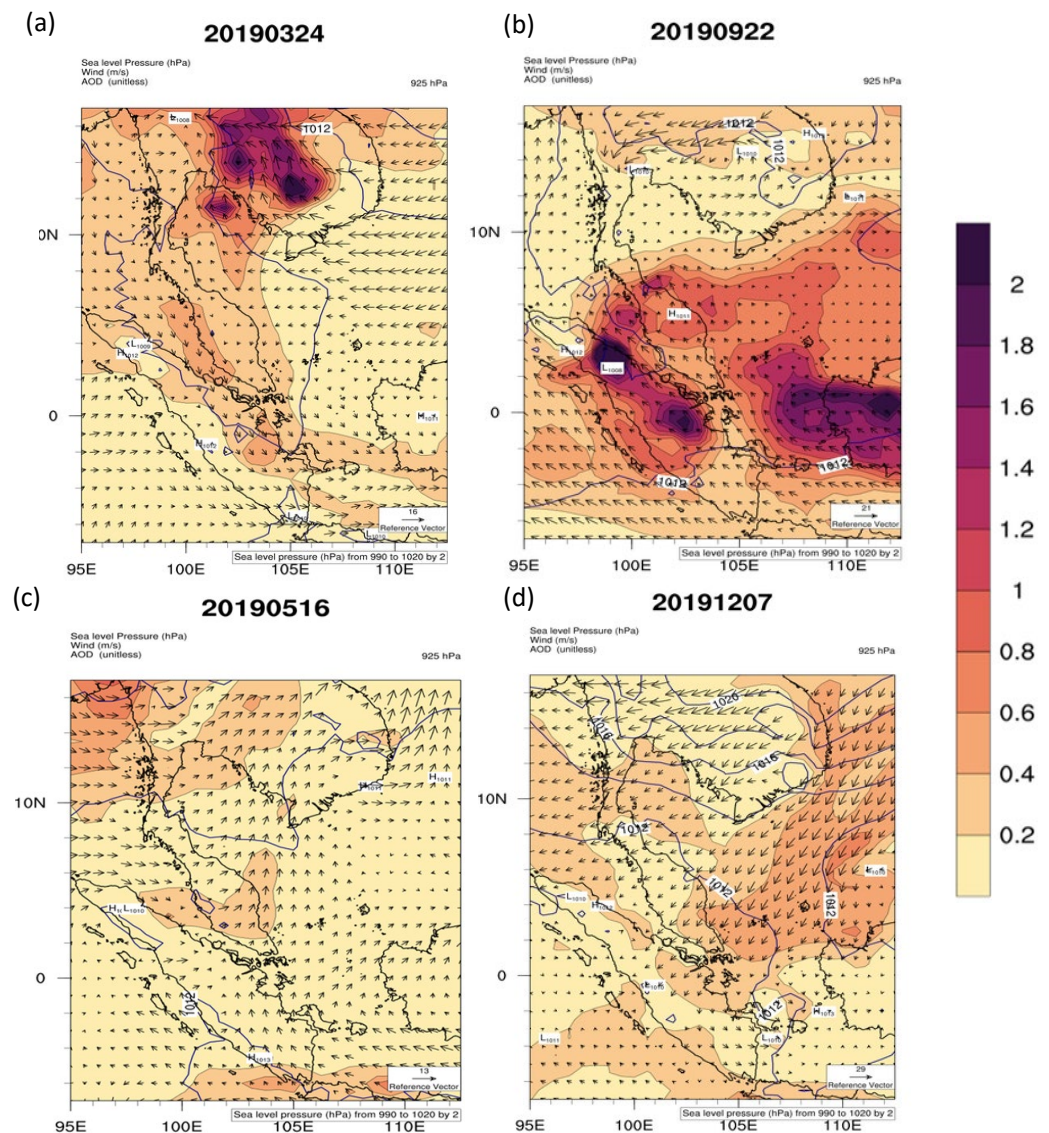
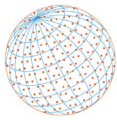
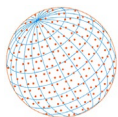


Fig. 4. The meteorological conditions of wind speed, wind direction, and sea level pressure versus AOD levels during (a) HP1, (b) HP2, (c) LP1, and (d) LP2.

from 0.01 to 0.3 as shown in Fig. 2. This is also supported by findings from Pani *et al.* (2018) which revealed that the mean AOD levels during low BB to extreme BB burning events in Thailand (closest country to the ECPM region) were between 0.6 to 2.50 when severe smoke episodes occurred in the Northern Peninsular Southeast Asia. Moreover, Yin *et al.* (2020) also stated that the AOD levels were below 0.3 when there were no BB activities occurring in 2015. Strong winds exceeding 10 m s^{-1} , supported by findings from Mohyeddin *et al.* (2020), either from the northeast or southwest of the ECPM with a high SLP at the upper and lower latitudes of the ECPM can push significant amounts of BB emissions towards the ECPM and decline its air quality. Additional information on the meteorological characteristics are provided in the supplementary Fig. S4. However, further studies are required to determine the extents to which local and non-local pollution can affect the ECPM region.

3.2 Identification of the Origin of Aerosols through the HYSPLIT Model

Trajectory analyses were used to identify the possible emission sources which influenced the $\text{PM}_{2.5}$ concentrations and AOD levels along the ECPM in 2019. The trajectory analyses for HP1 and HP2 were selected based on the time that the $\text{PM}_{2.5}$ concentrations exceeded the permissible limit of the NMAAQs as listed in Table 1. The LP1 and LP2 periods were selected based on the

**Table 1.** Detailed settings of the backward trajectory period.

		HP1	HP2	LP1	LP2
Backward tracing period		23–25 March	21–23 Sep.	15–17 May	6–8 Dec.
PM _{2.5} at Terengganu ($\mu\text{g m}^{-3}$)	Min	0.46	28.42	1.76	2.02
	Max	180.22	205.26	43.39	24.64
	Average	21.022	100.87	15.22	12.15
PM _{2.5} at Kelantan ($\mu\text{g m}^{-3}$)	Min	9.34	10.50	1.16	5.16
	Max	74.01	130.47	24.18	37.37
	Average	32.12	61.02	9.15	16.23
PM _{2.5} at Pahang ($\mu\text{g m}^{-3}$)	Min	19.89	26.76	8.63	5.32
	Max	51.41	133.53	70.46	33.81
	Average	19.51	98.91	23.83	12.34

lower values of PM_{2.5} concentrations and those within the permissible limit of the NMAAQs to act as a background for the local emissions indicators. The study further determined the types of aerosols suspended at different heights above the Earth's surface using CALIOP data. The identification of the types of aerosols within the atmosphere can help distinguish the dominant potential sources of air pollutants that influenced the air quality of the ECPM region during HP1, HP2, LP1, and LP2. The vertical feature mask attenuated backscatter at 532 nm was plotted to differentiate the aerosol types, followed by the profiling of tropospheric aerosol subtypes during HP1, HP2, LP1, and LP2 along the ECPM for daytime and nighttime.

3.2.1 High pollution period 1 (HP1)

The HP1 period coincided with the inter-monsoon season from the 19th of March until the 1st of May 2019 (MET, 2019). During HP1, the backward trajectory analysis showed that the aerosols were derived from the SCS and Indochina at all heights (Fig. 5 and Fig. S5 in the supplementary materials). On the 24th of March 2019, the analysis showed that the pollutant sources that influenced the ECPM region likely originated from Indochina, as supported by the high AOD values (Figs. 5(a) and 5(b)) located approximately at a 10°N–15°N latitude. The higher pressure in the northern part of the hemisphere, also known as the Siberian high associated with cold air masses, was still active towards the end of the boreal winter and managed to push the airmasses from the northern to the low-pressure southern part of Southeast Asia which is closer to the equator. Although the northeasterly winds during the inter-monsoon are not as strong as during the northeast monsoon, they can still help carry BB pollutants from upwind Indochina to the ECPM region (Mohyeddin *et al.*, 2020; Akhir *et al.*, 2014).

Figs. 5(a–d) illustrates the vertical feature mask and aerosol subtypes in the ECPM region (marked by red boxes) in the daytime and nighttime during HP1 and HP2 from CALIOP. The tropospheric aerosols detected were scattered at altitudes below 5 km throughout the day, with an additional layer at altitudes above 10 to 15 km in the nighttime during HP1, corresponding to the backward trajectory results shown in Fig. 5(b) since the emissions can only reach a height of 2.5 km. The tropospheric aerosols from polluted dust, dust, and polluted continental/haze were found to be scattered below 5 km in the daytime; during the nighttime, marine, polluted continental/haze, and elevated haze were found suspended below 5 km altitudes while the dust and elevated haze were scattered at altitudes within 10–15 km as shown in Figs. 6(b) and 6(d). The CALIPSO swath showed that the polluted and elevated smoke suspended at 5 km altitudes in the atmosphere were being transported from the northeast of the ECPM (Indochina) and degraded the air quality of the ECPM region.

3.2.2 High pollution period 2 (HP2)

The HP2 period coincided with the southeast monsoon period which occurred from the 2nd of May until the 24th of September 2019, the ENSO phenomenon (El-Niño) as it reported by MET, (2019), and with a drier condition with less precipitation, less cloud, prevailing westerly wind, and high outgoing long-wave radiation (Che *et al.*, 2019). The drier conditions provided conducive conditions for burning activities and increased the photochemical reactions of the pollutant for

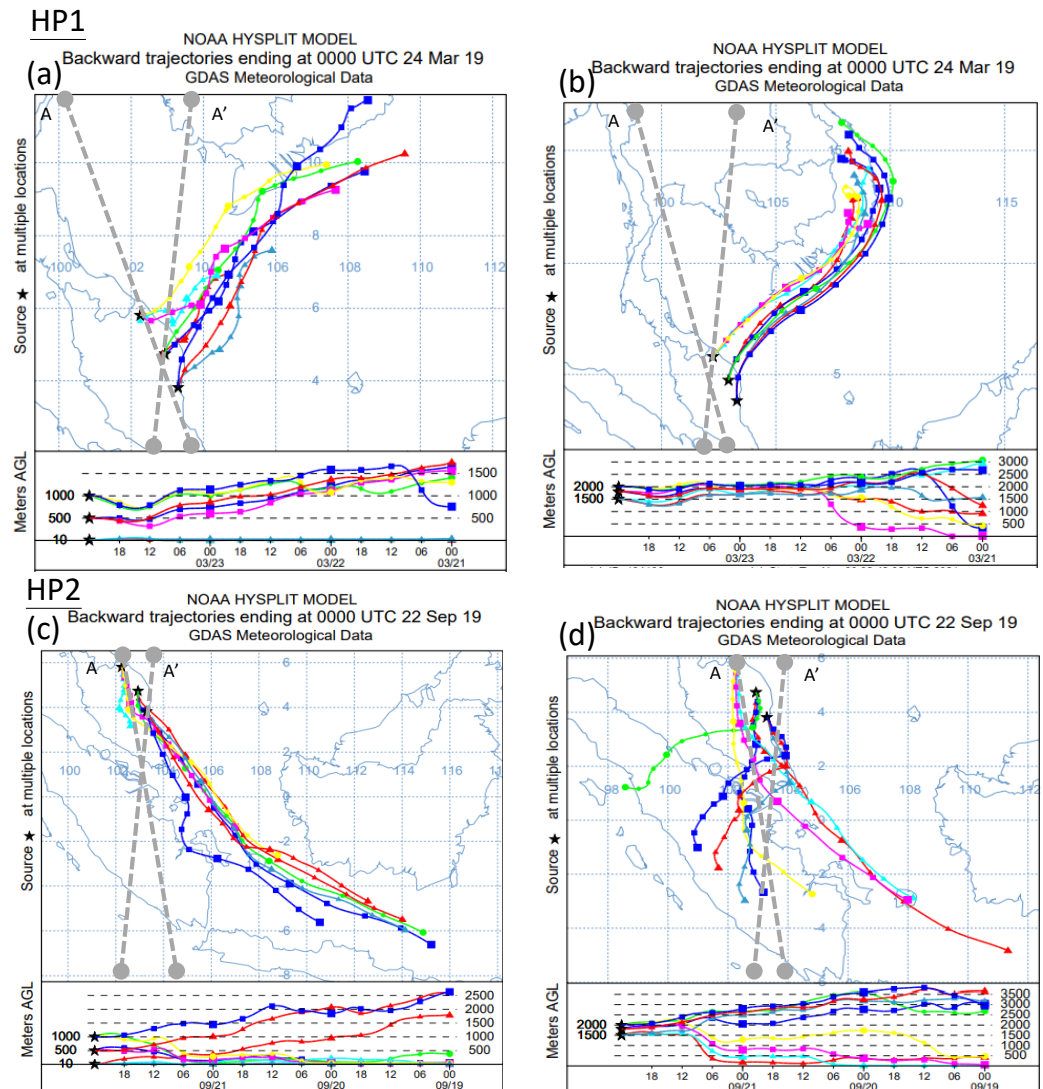
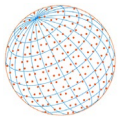


Fig. 5. Backward trajectories analyses at (a, c) 0–1000 m and (b, d) 1500–2000 m for HP1 (a, b) and HP2 (c, d) on three consecutive days with high PM_{2.5} concentrations in the ECPM region. The black dotted lines A (daytime) and A' (nighttime) are represent as a swath of CALIOP.

secondary aerosol formation in the atmosphere (Chenoli *et al.*, 2018; Wang *et al.*, 2016). Kanniah and Yaso (2010) concluded that low levels of seasonal rainfall, high relative ambient temperatures, together with southwesterly winds create a medium for the advection of air masses which contain BB-derived aerosols, especially from Kalimantan and Sumatra in Indonesia, triggering long-range pollutant transport to Malaysia's atmosphere.

For HP2, Fig. 5(c) shows that the emissions from the Karimata Strait (marked in Fig. 1(a)) and Kalimantan scattered at high altitudes before reaching the near-surface level of the ECPM region. Meanwhile, at altitudes of 1500 to 2000 m AGL, the pollutants were generated in Sumatra (21st and 22nd September 2019) and Kalimantan (23rd September 2019) (Fig. 5(c)). The sources were concurrent with significant AOD levels defined from MERRA-2 data at 5°S to 5°N and 100°E to 115°E. The presence of low precipitation, less clouds, high outgoing long-wave radiation, and southerly winds during the southwest monsoon initiated the horizontal transport of air masses that contained air pollutants from Sumatra and Kalimantan across the Malacca and Karimata straits to Peninsular Malaysia where they affected the air quality (Bucci *et al.*, 2020; Oozeer *et al.*, 2016). For more information on the sources of emissions during HP2, see Fig. S5.

The tropospheric aerosols were suspended at atmospheric altitudes below 5 km which agrees with the findings of the backward trajectory analyses as shown in Fig. 5(d), since the highest

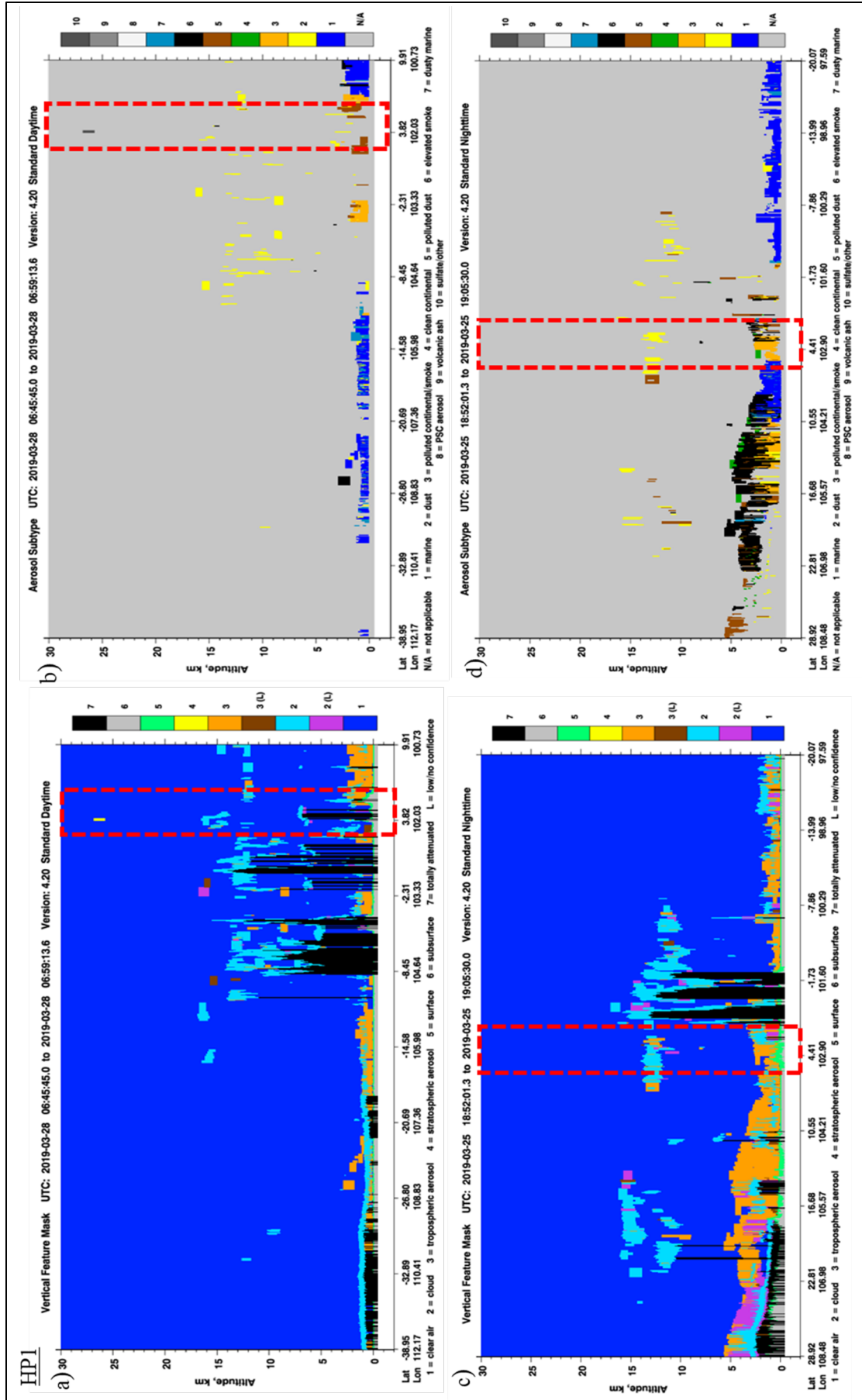


Fig. 6. CALIOP data of backscatter 532 nm cloud and aerosols in the ECMP regions during (a–d) HP1 and (e–h) HP2 for day and nighttime. The red dotted boxes show the areas that cover the ECMP regions.

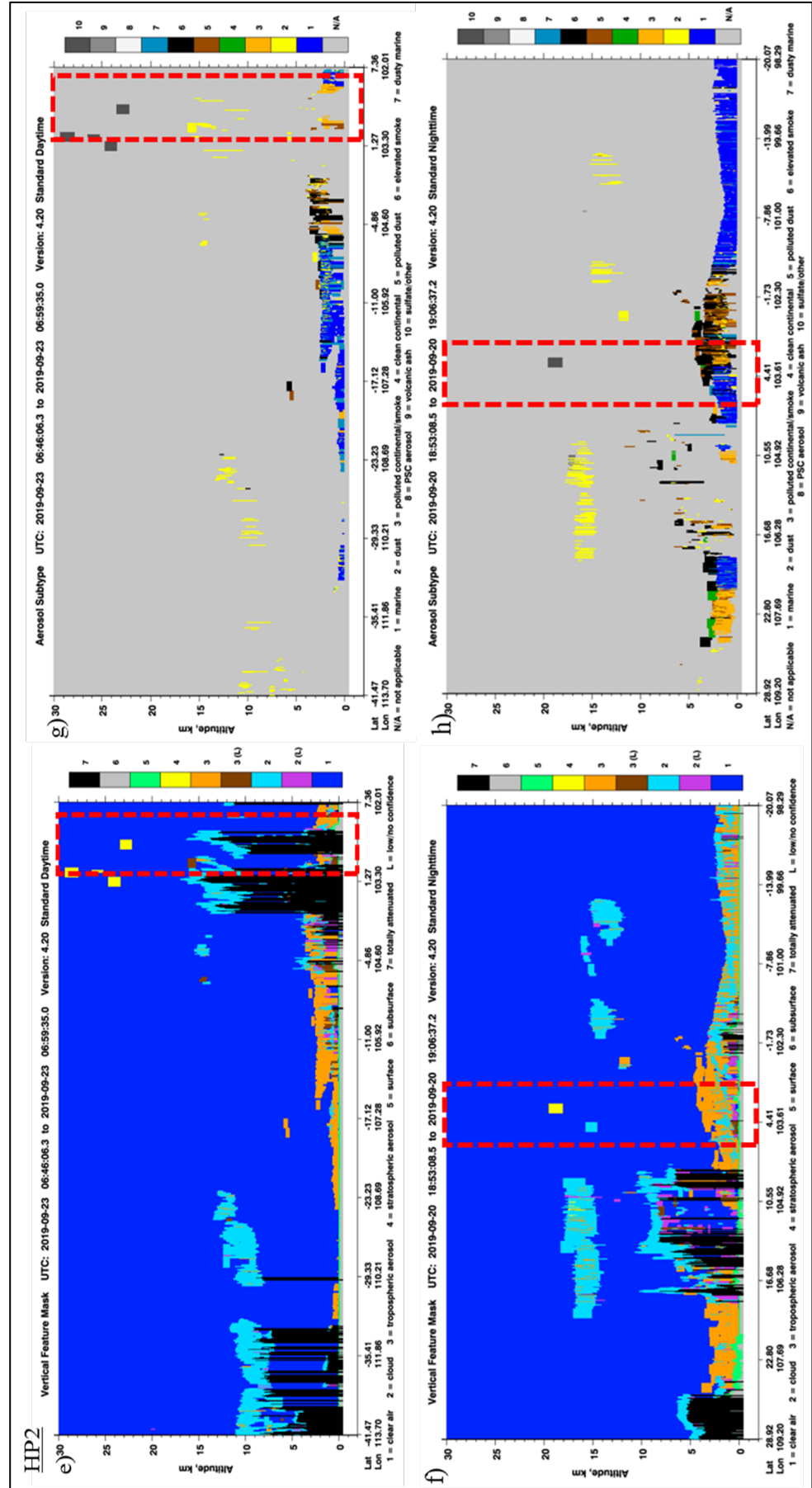
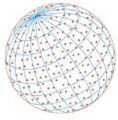


Fig. 6. (continued).



emissions were detected at 3.5 km altitudes; by having aerosol subtypes from marine, polluted continental/haze, and polluted dust sources observed in the daytime as shown in Figs. 6(e–f). In the nighttime, the troposphere aerosols were observed it scatter at below 5 km AGL together with marine, polluted continental/haze, elevated haze, and dust. Meanwhile, sulfate was found it scattered between 18 to 20 km AGL and considered a stratospheric aerosol (Figs. 6(g–h)). Hence, the CALIOP swaths obtained during the daytime and nighttime showed that the emissions of polluted smoke and elevated smoke suspended in the vertical aerosol profile originated from lower latitudes of the ECPM region and were travelling and engulfing the atmosphere of the ECPM region.

3.2.3 Low pollution period 1 (LP1)

The LP1 period was the transitional period of monsoonal changes or the end of the northeast monsoon period. For LP1, Figs. 7(a–b) show that the air masses passed through Singapore, the Strait of Johor, Strait of Malacca, and Sumatra. The emissions from the Strait of Johor, Singapore, and Strait of Malacca were significant at the near-surface level as shown in the supplementary Figs. S6(a–d). However, Fig. 7(b) shows that at 1500 to 2000 m AGL the emissions were originating from neighboring Sumatra, Indonesia. The ECPM region is considered to receive inputs from mixed sources of pollution, from local and non-local sources, that can influence the degradation of the air quality. The local emissions had a more significant effect on air quality than non-local emissions during this time. During LP1, the northern inter-tropical convergence zone (ITCZ) started to shift towards the south, and the low-polluted air masses carried from Sumatra by weak winds blew in emissions from BB (Dahari *et al.*, 2019; Andronache *et al.*, 2002).

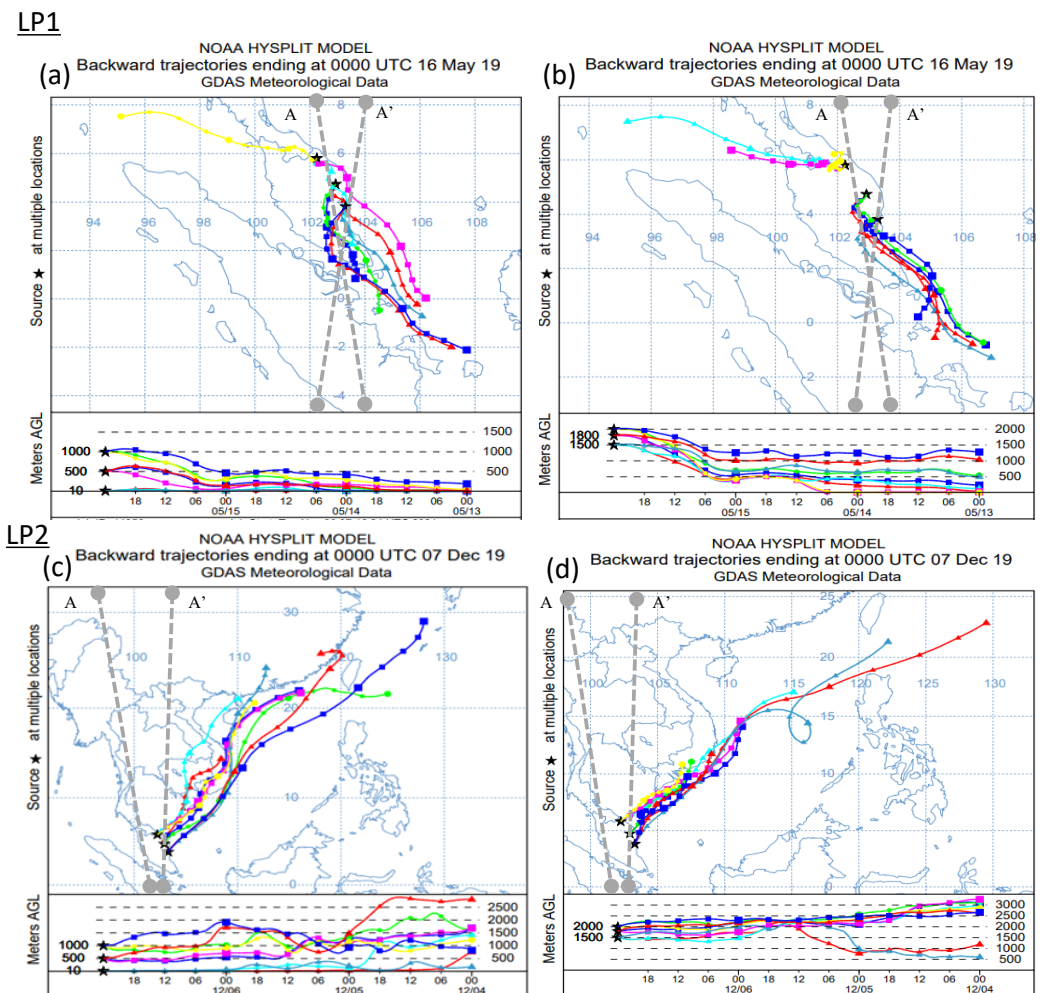


Fig. 7. Same as Fig. 5 but for the (a–b) LP1 and (c–d) LP2 periods.

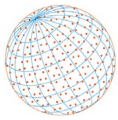


Fig. 8 shows the vertical distribution of aerosols during LP1 and LP2. These periods were considered as having a relatively clean atmosphere compared to HP1 and HP2. Some tropospheric aerosols that consisted of marine, dusty marine, and smoke pollutants were traced to altitudes below 2 km in the daytime and nighttime during LP1. The aerosols from dust and polluted dust were scattered at altitudes above 2 km at both times as shown in Figs. 8(a–d). The swath of CALIOP also shows that the clouds and suspended aerosols during LP1 were coming from the south of the ECPM region.

3.2.4 Low pollution period 2 (LP2)

For LP2, the trajectory analyses showed that the air masses were arriving from 500 m to 2000 m AGL from Indochina, China, and the SCS as shown in Fig. 6. The strong wind speeds with northeasterly directions and high SLP pushed the BB air masses to the ECPM region as shown in Fig. 4. Although the air masses were observed to originate from Indochina during LP2, the ECPM region experienced extremely heavy rainfall during the upcoming northeast monsoon season during LP2 with maximum values of rainfall of about 400 mm in December based on previous findings by *Fakaruddin et al. (2017)*. This condition prevented the air pollution from Indochina from reaching the ECPM region since the heavy rainfall had a negative correlation with the air pollutants, especially with particulate matter, because the pollutants were washed out along the transport pathway. This has been supported by previous findings from *Yassen and Jahi (2007)* which showed that the concentrations of total suspended solids in the air were decreasing as they were removed and washed out by the wet conditions during NEMs. Therefore, during the LP2 period, concurrent with the NEM, the atmosphere in November was generally clean. Fig. S6 provides more information on the trajectories analyses one day before and after the LP2. As expected, Figs. 8(e–h) show a relatively low significance of suspended tropospheric aerosols in the daytime and nighttime. Hence, the LP2 period showed the lowest significance of tropospheric aerosols in the atmosphere relative to HP1, HP2, and LP1, as it was correlated with the weather conditions experienced by the ECPM region as discussed earlier. Meanwhile, during LP2, the CALIOP swath also showed that clouds were dominating the atmosphere over suspended aerosols, as detected in the vertical aerosol profiling from the upper latitudes of the ECPM region.

3.3 Aerosol Species Contribution

The monthly aerosol species contribution to the ECPM region during the HP1, HP2, LP1, and LP2 periods were obtained from MERRA-2 model data. Figs. 8(a–g) show the distribution of aerosol species during HP1 and HP2. The results show that BC and OC had dominant contributions to the aerosol species during these two periods of time. During HP1, BC and OC were simultaneously present in significant levels in Indochina and the ECPM region. This is supported by the results of *Tsai et al. (2013)*, since the HP1 period also experienced the ‘Asian Brown Cloud’ that occurred between March and April in Indochina. The overflow of BB emissions during the Asian Brown Cloud events released large amounts of BC and OC to the SCS and the wind directions during the inter-monsoon may have had a great influence on the atmosphere of the ECPM.

Figs. 9(h–n) also show that the dominant aerosol species consisted of BC and OC which influenced the air quality in the ECPM region during HP2. It occurs simultaneously with the BB emissions from Sumatra and Kalimantan. The BB activities in Indonesia involved carbonaceous matter from slash and burning, open burning, wildfires, and others. The results agree with previous findings by *Latif et al. (2018)* and *Lee et al. (2018)* which showed that the BB that occurred in Kalimantan and Sumatra was dominated by emissions of OC and BC (estimated at about 50% for BC and 73% OC) in the form of particulate matter relative to local emissions. However, during both HP1 and HP2, the SO_4^{2-} values were also higher but most significant during LP1. Emissions of SO_4^{2-} are categorized as secondary aerosols which commonly relate with local emissions, specifically from natural and anthropogenic sources such as sea-spray, volcanoes, industrial activities, and transportation. Hence, further correlation analyses are needed to support the hypothesis that SO_4^{2-} was most significant due to local emissions during LP1.

The transitional monsoon period influenced the meteorological conditions during the LP1 period. The effects of the NEM were weaker than during HP1 as conditions had started to shift towards the SWM in May as mentioned in an annual report of 2019 from MET Malaysia. Hence,

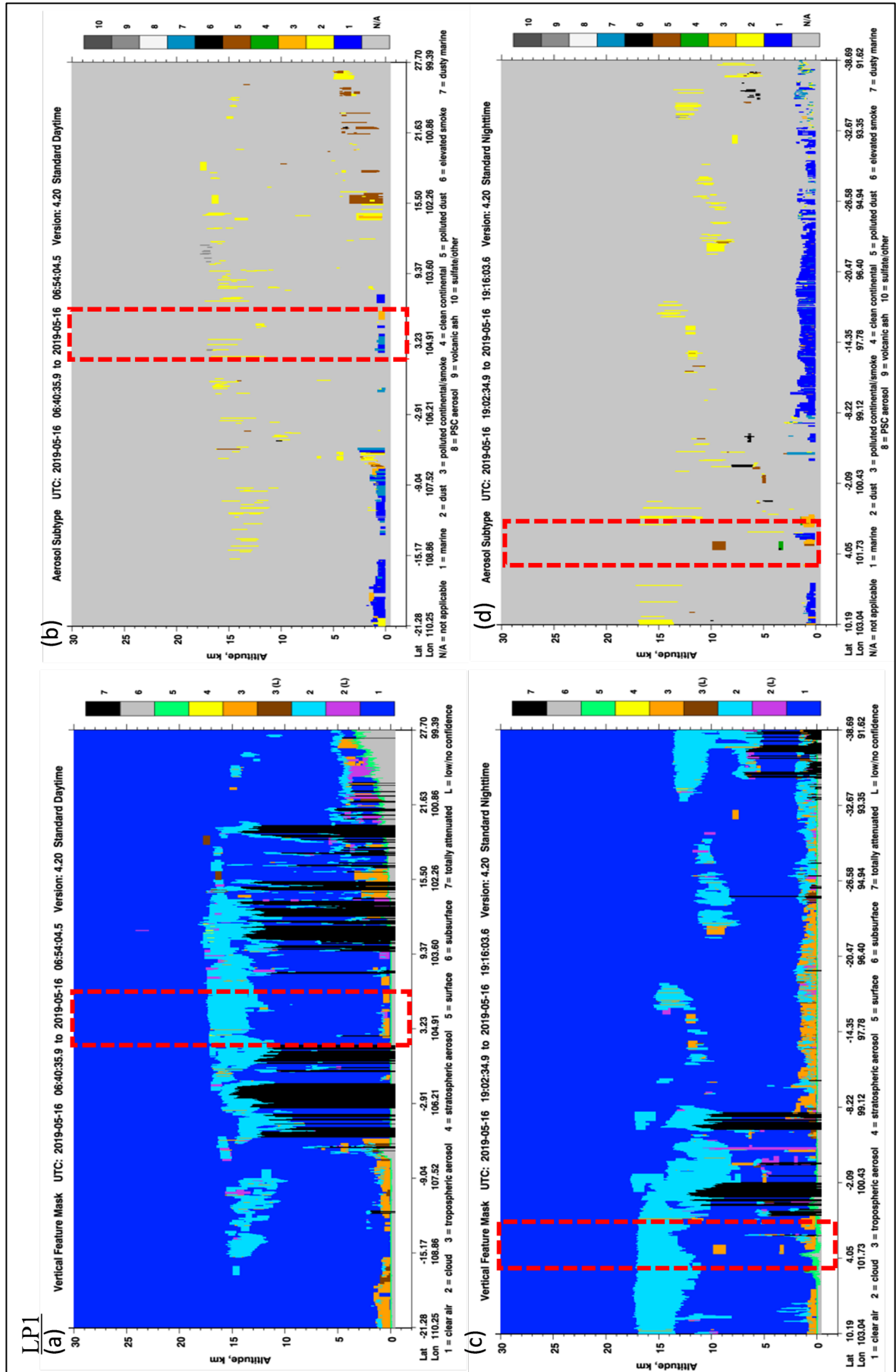


Fig. 8. Same as Fig. 6 but for the (a-d) LP1 and (e-h) LP2 periods.

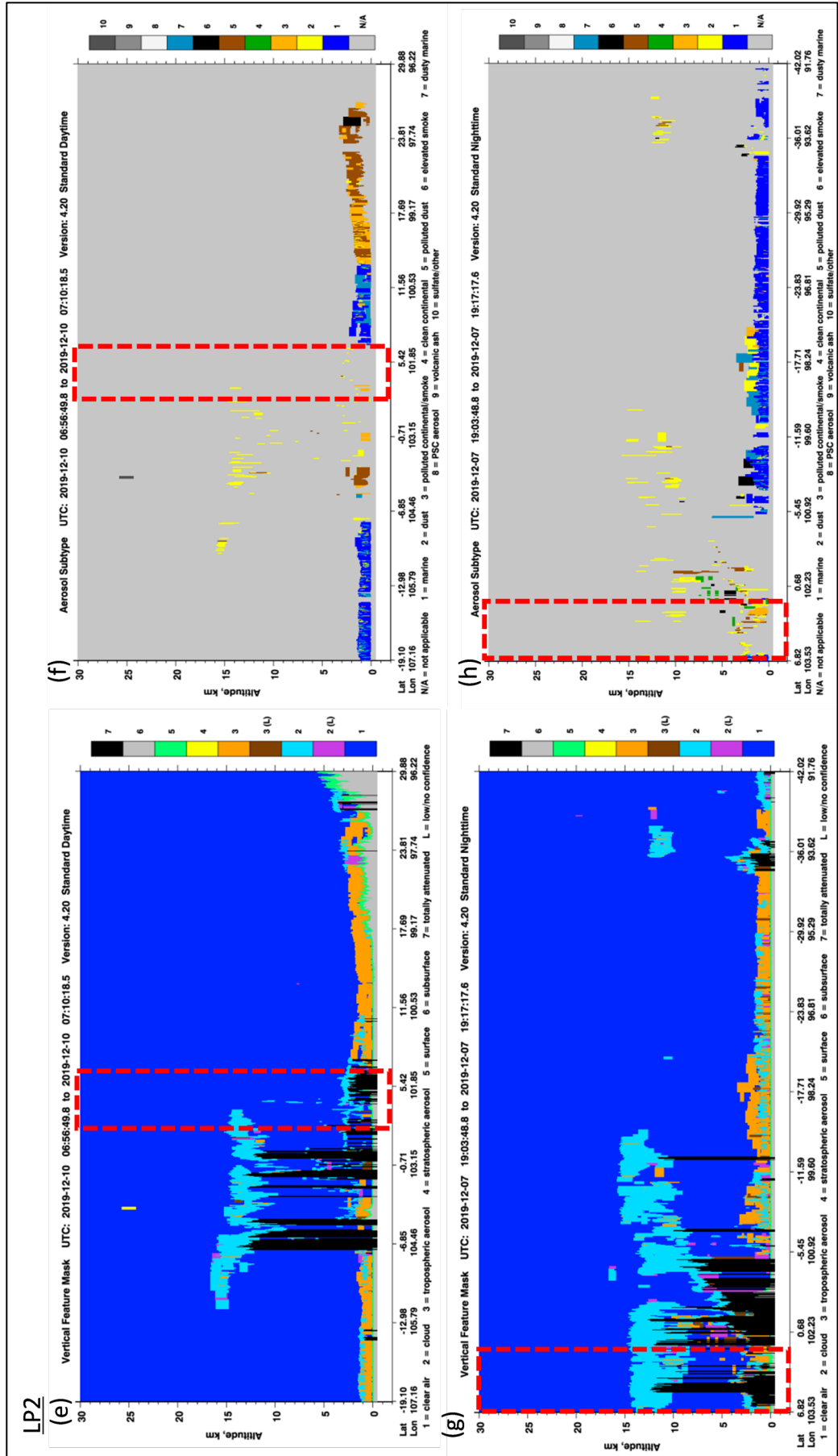
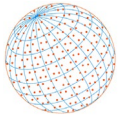
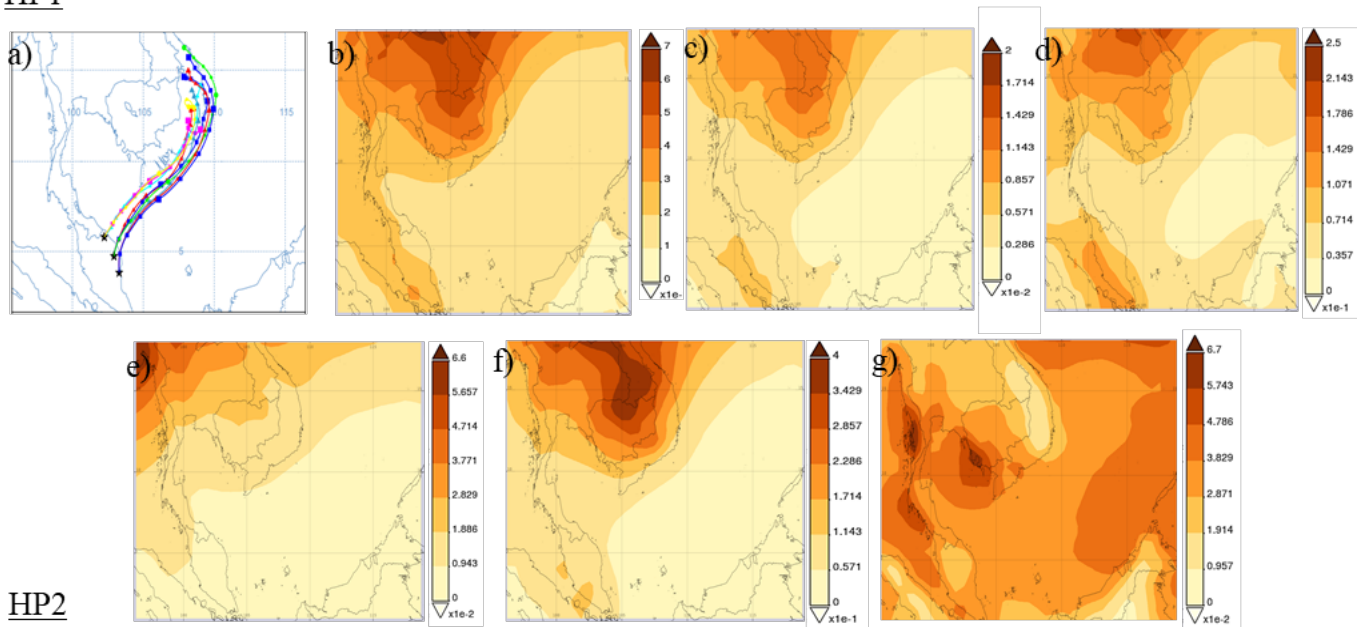


Fig. 8. (continued).



HP1



HP2

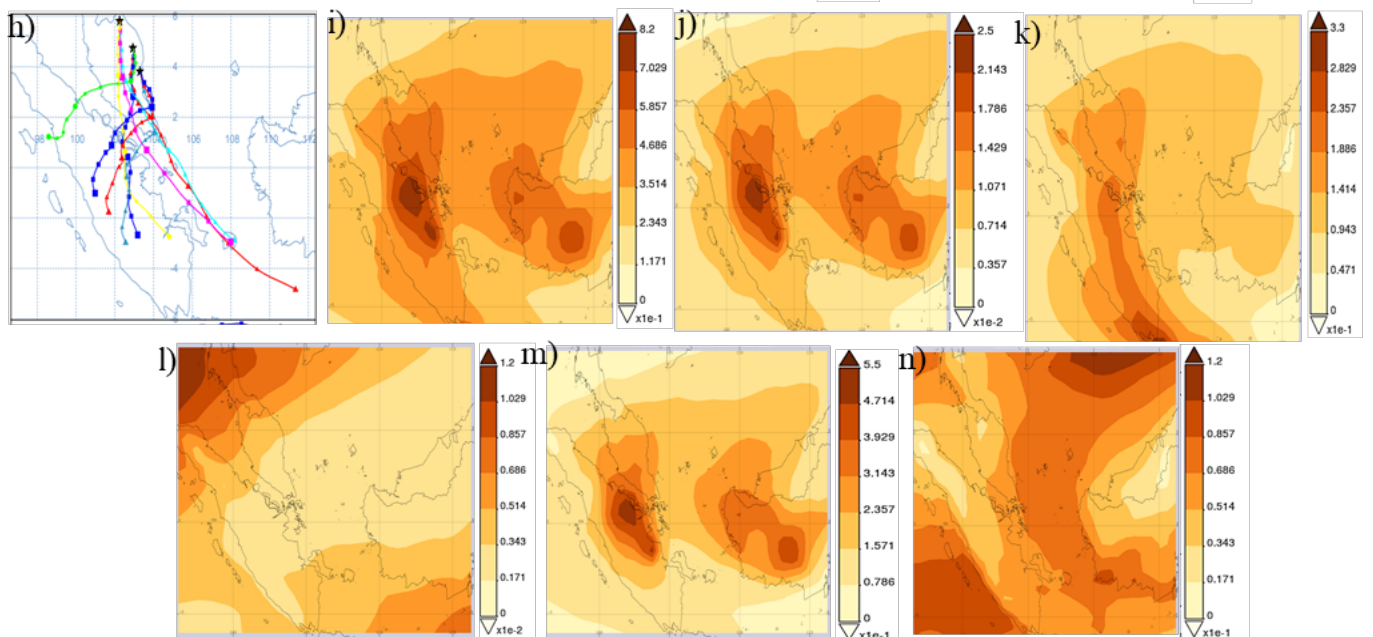
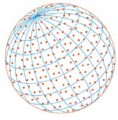
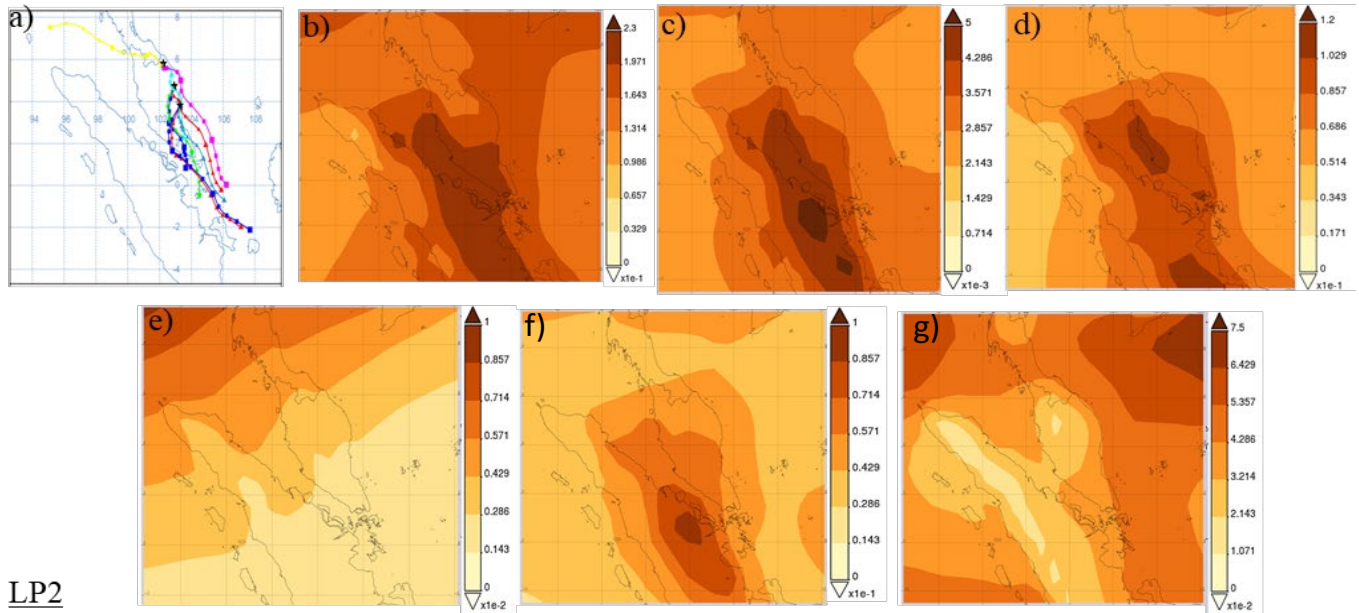


Fig. 9. The sources of contaminants that influenced the higher AOD levels in the ECPM in (a–g) HP1 and (h–n) HP2 MERRA-2 reanalysis data, with information on (a, h) the source of air masses, (b, i) AOD levels, (c, j) BC, (d, k) SO_4^{2-} , (e, l) dust, (f, m) OC, and (g, n) sea salt.

during this period, the weather conditions began to introduce drier ambient temperatures, low precipitation, and a shift of the winds blowing from northerly to western directions. According to Figs. 10(a–g), the high AOD levels were influenced by the mixed aerosol species which originated from local and non-local emissions from natural and anthropogenic activities; these were located in the south and north of Peninsular Malaysia which affected the air quality especially in the ECPM region during this time. Meanwhile during LP2, the air quality was influenced by the NEM weather conditions which were characterized by a high intensity of precipitation, high relative humidity, low temperatures, and cold winds blowing from the Siberian high, promoting wet conditions which lowered the AOD levels and all their species as shown in Figs. 10(h–n). Although the trajectory analysis showed that some emissions originated from Indochina during these periods, these did not influence the air quality in the ECPM region since all the pollutants from



LP1



LP2

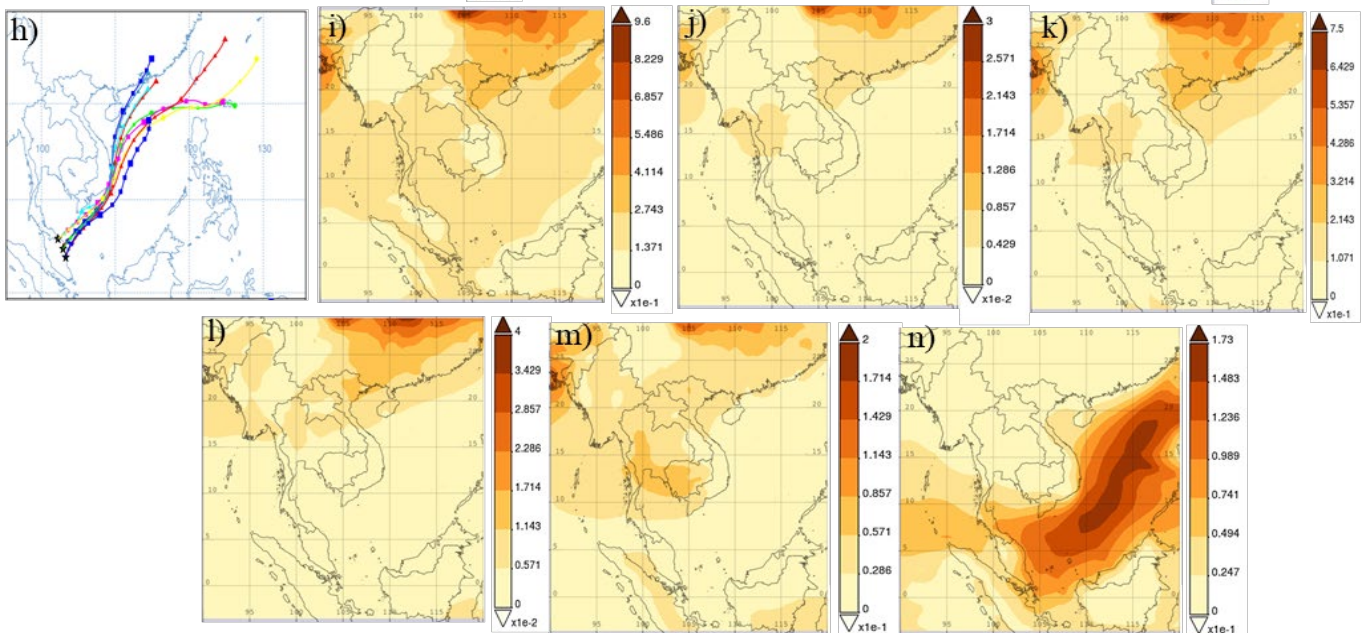
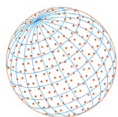


Fig. 10. The sources of contaminants that influenced the higher AOD levels in the ECPM in (a–g) LP1 and (h–n) LP2 MERRA-2 reanalysis data, with information on (a, h) the source of air masses, (b, i) AOD levels, (c, j) BC, (d, k) SO_4^{2-} , (e, l) dust, (f, m) OC, and (g, n) sea salt.

local and non-local sources had been washed out and deposited away by the heavy rains. Hence, this period can be considered as representing a clean atmospheric environment. As a result, this study focused on the HP1 and HP2 periods because the $\text{PM}_{2.5}$ concentrations and AOD levels were severe and exceeded the permissible limit defined by the DOE of Malaysia. An attempt was thus made at determining their sources, the long-range transport route of smoke events, and the types of aerosol species that dominated and degraded the air quality in the ECPM region due to its synoptic weather patterns.

3.3.1 Correlation analyses between AOD and aerosol species

The study continued to determine the relationship between AOD levels and the related aerosol species. The hourly AOD data from MERRA-2 analyses are not normally distributed as the

**Table 2.** Spearman bivariate correlation between AOD and BC, dust, OC, sea salt, and SO_4^{2-} during HP1, HP2, LP1, and LP2 in the ECPM region.

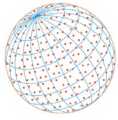
		AOD	BC	SO_4^{2-}	Dust	OC	Sea salt
HP1	AOD	1.00	0.908**	0.793**	0.499**	0.899**	0.520**
HP2	AOD	1.00	0.963**	0.614**	-0.100**	0.935**	0.442**
LP1	AOD	1.00	0.902**	0.942**	0.574**	0.833**	0.417**
LP2	AOD	1.00	0.329**	0.558**	0.660**	0.394**	0.457**

** Correlation is significant at the 0.01 level (2-tailed).

Kolmogorov-Smirnov and Shapiro-Wilk tests have $P(0.00) \leq 0.05$ and the normal distribution graph also skews to the left. In addition, the dataset does not have an equal variance as the Levene's test (homogeneous test) result is $P(0.00) \leq 0.05$. Since the data did not fulfill the requirements of both tests, it proceeded to the Kruskal-Wallis test. As a result, $P(0.00) \leq 0.05$ shows that the data have a significant difference of the median. Hence, because the data was non-parametric and not normally distributed, a Spearman bivariate correlation analysis was selected to determine the relationship between AOD and the aerosol species during two different periods in the ECPM region.

Table 2 shows the Spearman bivariate correlation results for the four pollution periods. The relationships of AOD with BC, SO_4^{2-} , dust, OC, and sea salt were determined. The relationship of AOD with the other aerosol species in the ECPM region during different periods can be summarized as BC > OC > SO_4^{2-} > sea salt > dust during HP1, BC > OC > SO_4^{2-} > sea salt > dust during HP2, and SO_4^{2-} > BC > OC > dust > sea salt during LP1. The LP2 period is not discussed since this period had low pollution levels with a minimal influence from BB emissions because it experienced the NEM associated with wet conditions as explained in Section 3.2.4. Aerosol species, especially from BC, OC, and SO_4^{2-} , influenced the AOD levels in the same way during both HP1 and HP2. Indeed, the BC, OC, and SO_4^{2-} pollutants had strong and positive relationship with AOD during HP1 and HP2: BC ($r = 0.908$, $p < 0.01$), OC ($r = 0.899$, $p < 0.01$), and SO_4^{2-} ($r = 0.793$, $p < 0.01$) during HP1, and BC ($r = 0.963$, $p < 0.01$), OC ($r = 0.935$, $p < 0.01$), and SO_4^{2-} ($r = 0.614$, $p < 0.01$) during HP2. Meanwhile, during LP1 the SO_4^{2-} ($r = 0.942$, $p < 0.01$), BC ($r = 0.902$, $p < 0.01$), OC ($r = 0.833$, $p < 0.01$), and dust ($r = 0.574$, $p < 0.574$) levels showed strong positive correlation, and sea salt ($r = 0.417$, $p < 0.417$) a moderately positive relationship with AOD levels.

The correlation analysis results support the findings presented in Section 3.3, showing significant levels of BC and OC during HP1 and HP2. Due to favorable weather conditions, the air quality was degraded by dominant sources of aerosol species from large amounts of BB emissions from Indochina (during HP1) and Indonesia (during HP2). Khoir *et al.* (2021) estimated an average of more than 25000 fire hotspots in Indochina during March and April and more than 2000 from August to September of 2015 based on data from 2001 to 2021. These findings support the hypothesis that BB had a greater impact than local emissions on the air quality of the ECPM region based on the large number of fire hotspots detected. Black carbon, also known as elemental carbon, and OC, was released from BB, fossil fuels, and secondary organic aerosol residues. Both were released into the atmosphere as fine and coarse particulate matter. The combustion of carbonaceous material during BB resulted in significant levels of BC and OC. The results reported by Engling *et al.* (2014) proved that BC and OC comprised about 50% in total suspended particles during hazy days compared to 25% during non-hazy days. The BC released by BB was coated with organic materials. Meanwhile, local emissions such as those from urban activities coated the BC primarily with SO_4^{2-} , nitrate, and primary and secondary OC (Qi and Wang, 2019). During the LP1 period, when non-local and local emissions were mixed, SO_4^{2-} had the strongest correlation with AOD levels. The formation of SO_4^{2-} involves photochemical and oxidation reactions which mainly take place in the industrial sector, and in biogenic and natural sources. However, BB emission has a minor influence on secondary inorganic carbon which it released depends on the type of residual, soil, and other factors involved (Latif *et al.*, 2018; Chen *et al.*, 2017; Behera and Balasubramanian, 2014). Previous studies by Zainal *et al.* (2021) and Lee *et al.* (2018) showed that about 93% of atmospheric SO_4^{2-} was derived from non-fire events and that it was present in higher concentrations during pre-smoke events than during smoke events and post-smoke events that occurred in year 2019 in Malaysia. In Terengganu, the higher correlation of SO_4^{2-} with high AOD levels and $\text{PM}_{2.5}$ concentrations during LP1 can be attributed to the large-scale emissions from the petroleum sector



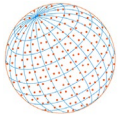
(main economic sector) which affect the air quality in the ECPM region (Ragothaman and Anderson, 2017). During HP1 and HP2, the BC and OC levels were directly proportional to the level of AOD and ambient PM_{2.5} concentrations in the ECPM region, in large part due to BB activities. Meanwhile, due to the complicated chemical reactions of SO₄²⁻, it is reasonable to assume that the SO₄²⁻ derived from both local and non-local sources, which originated primarily from fossil fuel combustion.

In summary, according to the HYSPLIT trajectory analyses, the high ambient PM_{2.5} concentrations and AOD levels during the HP1 period resulted from intense BB activities in the northeast of the ECPM region (Indochina) while the HP2 period was influenced by BB activities located in the southwest (Indonesia). Inter-monsoon and SWM weather conditions influenced the transport route of transboundary smoke in Indochina and Indonesia during HP1 and HP2. The air quality was influenced by mixed emissions from local and non-local sources during LP1. Meanwhile, LP2 was found to have the cleanest environment out of all studied periods as it experienced the NEM which helped wash out the pollutants and deposit them away from the area. Therefore, BC, OC, and SO₄²⁻ had a strong positive influence on AOD levels and ambient PM_{2.5} concentrations during HP1 and HP2. However, SO₄²⁻ levels were more significant during LP1 due to the complex chemical reactions involving SO₄²⁻ in local emission sources. Understanding the complex interactions between aerosol properties, the microphysical state of the atmosphere can help gain crucial information on the behavior of the aerosols themselves and should be considered in future studies to gain a better insight into the long-range transport of air pollutants. Moreover, aerosol species of nitrate also should be included in future studies to see how significant it is in influencing the PM_{2.5} concentration and AOD level, especially during BB in ECPM region.

4 CONCLUSIONS

In conclusion, the hourly trend of PM_{2.5} concentrations and AOD levels in the ECPM regions (Terengganu, Kelantan, and Pahang) in 2019 revealed two significant peaks of high pollution events. Hence, four different pollution periods with high and low PM_{2.5} concentration trends and AOD levels in March–April (HP1), August–September (HP2), May (LP1), and December (LP2) were identified to determine the sources of high PM_{2.5} concentrations and AOD levels in the studied regions. Both high and low concentrations of PM_{2.5} and AOD levels were observed through HYSPLIT backward trajectory and CALIOP data analyses. High concentrations of PM_{2.5} and AOD levels potentially originated from and were influenced by BB in Indochina during HP1, burning activities in Kalimantan and Sumatra during HP2, local (natural and anthropogenic activities) and non-local emissions during LP1, and natural sources during LP2. During HP1, the tropospheric aerosols were scattered below 5 km altitudes in the daytime meanwhile at nighttime, the tropospheric aerosols were scattered at two different heights which were at 5 km and between 10 and 15 km. The tropospheric aerosols in HP2 were scattered below 5 km (day- and nighttime). During LP1, the tropospheric aerosols were observed at two different heights which were below 2 km and around 12–13 km during daytime, and at nighttime it scattered at three different atmosphere altitudes which were 2 km, 3–4 km, and 9–10 km. The levels of tropospheric aerosols in LP2 were relatively low and did not become the main concern in this study because it's likely they would be deposited in the atmosphere.

The Spearman bivariate correlation analysis results showed that the AOD levels during the HP1 and HP2 periods were most influenced by BC, followed by OC, SO₄²⁻, sea salt, and dust. During LP1, SO₄²⁻ exerted the strongest influence on AOD levels, followed by BC, OC, dust, and sea salt. The BC, OC, and SO₄²⁻ levels, especially during HP1, HP2, and LP1, showed a strong positive correlation with AOD levels and PM_{2.5} concentrations. Relative to HP1 and HP2, the SO₄²⁻ levels had a significant effect on the AOD levels during LP1. This study obtained important data on the sources of pollutant emissions during various polluted episodes, as well as the types of aerosol species that influence the air quality in ECPM regions. These results can help guide policymakers and develop monitoring measures to protect the air quality of the ECPM. Further research into the behavior of aerosols and their interactions at different atmospheric altitudes during different monsoon seasons in Malaysia is needed to better understand how aerosols are transported over long-range routes.



ACKNOWLEDGMENTS

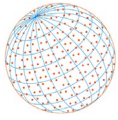
We gratefully acknowledge the Ministry of Higher Education (MoHE) Malaysia (FRGS/1/2020/WAB02/UKM/02/1) and Shanghai International Science and Technology Cooperation (NO. 19230742500) for supporting and funding this work. All authors would like to express gratitude for the provision of MODIS, CALIOP, and MERRA-2 data from NASA, the weather data from Malaysian Meteorological Department (MET), and the air quality data from the Department of Environment (DOE) Malaysia.

SUPPLEMENTARY MATERIAL

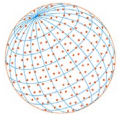
Supplementary material for this article can be found in the online version at <https://doi.org/10.4209/aaqr.210393>

REFERENCES

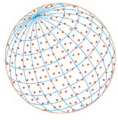
- Akhir, M.F., Zakaria, N.Z., Tangang, F. (2014). Intermonsoon variation of physical characteristics and current circulation along the East Coast of Peninsular Malaysia. *Int. J. Oceanogr.* 2014, 1–9. <https://doi.org/10.1155/2014/527587>
- Andronache, C., Donner, L.J., Seman, C.J., Hemler, R.S. (2002). A study of the impact of the Intertropical Convergence Zone on aerosols during INDOEX. *J. Geophys. Res.* 107, 8027. <https://doi.org/10.1029/2001JD900248>
- Ashfold, M.J., Latif, M.T., Samah, A.A., Mead, M.I., Harris, N.R.P. (2017). Influence of Northeast Monsoon cold surges on air quality in Southeast Asia. *Atmos. Environ.* 166, 498–509. <https://doi.org/10.1016/j.atmosenv.2017.07.047>
- Azhari, A., Halim, N.D.A., Mohtar, A.A.A., Aiyub, K., Latif, M.T., Ketznel, M. (2021). Evaluation and prediction of PM₁₀ and PM_{2.5} from road source emissions in Kuala Lumpur City Centre. *Sustainability* 13, 5402. <https://doi.org/10.3390/su13105402>
- Behera, S.N., Balasubramanian, R. (2014). Influence of biomass burning on temporal and diurnal variations of acidic gases, particulate nitrate, and sulfate in a tropical urban atmosphere. *Adv. Meteorol.* 2014, 828491. <https://doi.org/10.1155/2014/828491>
- Bucci, S., Legras, B., Sellitto, P., D'Amato, F., Viciani, S., Montori, A., Chiarugi, A., Ravegnani, F., Ulanovsky, A., Cairo, F., Stroh, F. (2020). Deep convective influence on the UTLS composition in the Asian Monsoon Anticyclone region: 2017 StratoClim campaign results. *Atmos. Chem. Phys.* 20, 12193–12210. <https://doi.org/10.5194/acp-2019-1053>
- Che, H., Gui, K., Xia, X., Wang, Y., Holben, B.N., Goloub, P., Cuevas-Agulló, E., Wang, H., Zheng, Y., Zhao, H., Zhang, X. (2019). Large contribution of meteorological factors to inter-decadal changes in regional aerosol optical depth. *Atmos. Chem. Phys.* 19, 10497–10523. <https://doi.org/10.5194/acp-19-10497-2019>
- Chen, J., Li, C., Ristovski, Z., Milic, A., Gu, Y., Islam, M. S., Wang, S., Hao, J., Zhang, H., He, C., Guo, H., Fu, H., Miljevic, B., Morawska, L., Thai, P., Lam, Y.F., Pereira, G., Ding, A., Huang, X., Dumka, U.C. (2017). A review of biomass burning: Emissions and impacts on air quality, health and climate in China. *Sci. Total Environ.* 579, 1000–1034. <https://doi.org/10.1016/j.scitotenv.2016.11.025>
- Chenoli, S.N., Jayakrishnan, P.R., Samah, A.A., Hai, O.S., Ahmad Mazuki, M.Y., Lim, C.H. (2018). Southwest monsoon onset dates over Malaysia and associated climatological characteristics. *J. Atmos. Sol. Terr. Phys.* 179, 81–93. <https://doi.org/10.1016/j.jastp.2018.06.017>
- Dahari, N., Muda, K., Hussein, N., Latif, M.T., Khan, M.F., Mohamad Khir, M.S. (2019). Long-range transport and local emission of atmospheric PM_{2.5} in Southern Region of Peninsular Malaysia. *IOP Conference Series: Mater. Sci. Eng. C* 636, 012005. <https://doi.org/10.1088/1757-899X/636/1/012005>
- Department of Environment, Malaysia (DOE) (2021). Air and Haze Quality Report in Malaysia. https://enviro2.doe.gov.my/ekmc/years/2019/?s=Laporan+kualiti+udara&post_types=digital-content (accessed 11 August 2021).



- Engling, G., He, J., Betha, R., Balasubramanian, R. (2014). Assessing the regional impact of Indonesian biomass burning emissions based on organic molecular tracers and chemical mass balance modeling. *Atmos. Chem. Phys.* 14, 8043–8054. <https://doi.org/10.5194/acp-14-8043-2014>
- Fakaruddin, F.J., Sang, Y.W., Mat Adam, M.K., Chang, N., Abdullah, M.H. (2017). Analysis of the Northeast Monsoon 2016/2017. Malaysian Meteorological Department, Malaysia. https://www.met.gov.my/data/research/researchpapers/2017/researchpaper_201701.pdf
- Forster, P., Ramaswamy, V., Artaxo, P., Berntsen, T., Betts, R., Fahey, D.W., Haywood, J., Lean, J., Lowe, D.C., Myhre, G., Nganga, J., Prinn, R., Raga, G., Schulz, M., Van Dorland, R. (2007). Changes in Atmospheric Constituents and in Radiative Forcing. in: *Climate Change 2007: The Physical Science Basis. Contribution of Working Group I to the Fourth Assessment Report of the Intergovernmental Panel on Climate Change*. Solomon, S., Qin, D., Manning, M., Chen, Z., Marquis, M., Averyt, K.B., Tignor, M., Miller, H.L. (Eds.), Cambridge University Press, Cambridge, United Kingdom and New York, NY, USA. <https://www.ipcc.ch/site/assets/uploads/2018/02/ar4-wg1-chapter2-1.pdf>
- Hatzianastassiou, N., Matsoukas, C., Drakakis, E., Stackhouse, P.W., Koepke, P., Fotiadis, A., Pavlakis, K.G., Vardavas, I. (2007). The direct effect of aerosols on solar radiation based on satellite observations, reanalysis datasets, and spectral aerosol optical properties from Global Aerosol Data Set (GADS). *Atmos. Chem. Phys.* 7, 2585–2599. <https://doi.org/10.5194/acp-7-2585-2007>
- Hatzianastassiou, N. (2009). The direct effect of aerosols on the radiation budget and climate of the Earth-atmosphere system: its variability in space and time. EGU General Assembly 2009, Vienna, Austria. p. 10109.
- He, J., He, R., Zhang, Y. (2018). Impacts of air-sea interactions on regional air quality predictions using a coupled atmosphere-ocean model in southeastern U.S. *Aerosol Air Qual. Res.* 18, 1044–1067. <https://doi.org/10.4209/aaqr.2016.12.0570>
- Hee, W.S., Lim, H.S., Jafri, M.Z.M., Lolli, S., Ying, K.W. (2016). Vertical profiling of aerosol types observed across monsoon seasons with a Raman Lidar in Penang Island, Malaysia. *Aerosol Air Qual. Res.* 16, 2843–2854. <https://doi.org/10.4209/aaqr.2015.07.0450>
- Huang, H., Gu, Y., Xue, Y., Jiang, J., Zhao, B. (2019). Assessing aerosol indirect effect on clouds and regional climate of East/South Asia and West Africa using NCEP GFS. *Clim. Dyn.* 52, 5759–5774. <https://doi.org/10.1007/s00382-018-4476-9>
- IPCC (2013). *Climate change 2013: The physical science basis Contribution of working Group I to the fifth assessment report of the intergovernmental panel on climate change*. Cambridge University Press, Cambridge.
- Jacobson, M.Z. (2014). Effects of biomass burning on climate, accounting for heat and moisture fluxes, black and brown carbon, and cloud absorption effects. *J. Geophys. Res.* 3, 6578–6595. <https://doi.org/10.1002/2014JD021861>
- Kanniah, K.D., Yaso, N. (2010). Preliminary Analysis of the spatial and temporal pattern of aerosols and their Impact on climate in Malaysia using MODIS satellite data. *International Archives of the Photogrammetry, Remote Sensing and Spatial Information Science, Volume XXXVIII, Part 8, Kyoto Japan 2010*, pp. 386–391.
- Khoir, A.N., Ooi, M.C.G., Liew, J., Suradi, Kurniawan, A., Ni'amillah, A. (2021). MODIS-derived fire spatial and temporal distribution during haze season in Southeast Asia using empirical orthogonal function. *IOP Conf. Ser.: Earth Environ. Sci.* 880, 012003. <https://doi.org/10.1088/1755-1315/880/1/012003>
- Kok, P.H., Akhir, M.F., Tangang, F.T. (2015). Thermal frontal zone along the east coast of Peninsular Malaysia. *Cont. Shelf Res.* 110, 1–15. <https://doi.org/10.1016/j.csr.2015.09.010>
- Latif, M.T., Othman, M., Idris, N., Juneng, L., Abdullah, A.M., Hamzah, W.P., Khan, M.F., Nik Sulaiman, N.M., Jewaratnam, J., Aghamohammadi, N., Sahani, M., Xiang, C.J., Ahamad, F., Amil, N., Darus, M., Varkkey, H., Tangang, F., Jaafar, A.B. (2018). Impact of regional haze towards air quality in Malaysia: A review. *Atmos. Environ.* 177, 28–44. <https://doi.org/10.1016/j.atmosenv.2018.01.002>
- Lee, H.H., Iraqui, O., Gu, Y., Yim, S.H.L., Chulakadabba, A., Tonks, A.Y.M., Yang, Z., Wang, C. (2018). Impacts of air pollutants from fire and non-fire emissions on the regional air quality in Southeast Asia. *Atmos. Chem. Phys.* 18, 6141–6156. <https://doi.org/10.5194/acp-18-6141-2018>



- Liu, B., Ma, Y., Gong, W., Zhang, M., Wang, W., Shi, Y. (2018). Comparison of AOD from CALIPSO, MODIS, and sun photometer under different conditions over Central China. *Sci. Rep.* 8, 10066. <https://doi.org/10.1038/s41598-018-28417-7>
- Liu, X., Zhang, Y.-L., Peng, Y., Xu, L., Zhu, C., Cao, F., Zhai, X., Haque, M.M., Yang, C., Chang, Y., Huang, T., Xu, Z., Bao, M., Zhang, W., Fan, M., Lee, X. (2019). Chemical and optical properties of carbonaceous aerosols in Nanjing, eastern China: Regionally transported biomass burning contribution. *Atmos. Chem. Phys.* 19, 11213–11233. <https://doi.org/10.5194/acp-19-11213-2019>
- Malaysian Meteorological Department, Malaysia (MET) (2019). Annual Report of Malaysian Meteorological Department. Malaysian Meteorological Department, Malaysia. <https://www.met.gov.my>
- Mohyeddin, N., Samah, A.A., Chenoli, S.N., Ashfold, M.J., Mead, M.I., Oram, D., Latif, M.T., Sivaprasad, P., Mohd Nor, M.F.F. (2020). The effects of synoptic and local meteorological condition on CO₂, CH₄, PM₁₀ and PM_{2.5} at Bachok Marine Research Station (BMRS) in Peninsular Malaysia. *Meteorol. Atmos. Phys.* 132, 845–868. <https://doi.org/10.1007/s00703-020-00724-7>
- Morgan, W.T., Allan, J.D., Bauguitte, S., Darbyshire, E., Flynn, M.J., Lee, J., Liu, D., Johnson, B., Haywood, J., Longo, K.M., Artaxo, P.E., Coe, H. (2020). Transformation and ageing of biomass burning carbonaceous aerosol over tropical South America from aircraft in situ measurements during SAMBBA. *Atmos. Chem. Phys.* 20, 5309–5326. <https://doi.org/10.5194/acp-20-5309-2020>
- National Oceanic and Atmospheric Administration (NOAA) (2021a). National Air Resource Laboratory, HYSPLIT Trajectory Model. https://www.ready.noaa.gov/HYSPLIT_traj.php (accessed 15 July 2021).
- National Oceanic and Atmospheric Administration (NOAA) (2021b). National Air Resource Laboratory, HYSPLIT Trajectory Model. <https://www.ready.noaa.gov/hypub/limitations.html> (accessed 10 August 2021).
- Nowottnick, E.P., Colarco, P.R., Welton, E.J., Da Silva, A. (2015). Use of the CALIOP vertical feature mask for evaluating global aerosol models. *Atmos. Meas. Tech.* 8, 3647–3669. <https://doi.org/10.5194/amt-8-3647-2015>
- Ooi, S.H., Samah, A.A., Braesicke, P. (2011). A case study of the Borneo Vortex genesis and its interactions with the global circulation. *J. Geophys. Res.* 116, D21116. <https://doi.org/10.1029/2011JD015991>
- Oozer, M.Y., Chan, A., Chel-Gee Ooi, M., Zazur, A.M., Salinas, S.V., Chew, B.N., Morris, K.I., Choong, W.K. (2016). Numerical study of the transport and convective mechanisms of biomass burning haze in South-Southeast Asia. *Aerosol Air Qual. Res.* 16, 2950–2963. <https://doi.org/10.4209/aaqr.2015.07.0461>
- Pakar Scieno TW Sdn Bhd (PSTW) (2018a). Standard operational procedure for continuous air quality monitoring (CAQM). operation, scheduled maintenance, troubleshooting.
- Pakar Scieno TW Sdn Bhd (PSTW) (2018b). Standard operational procedure for continuous air quality monitoring (CAQM) data validation.
- Pani, S.K., Lin, N.H., Chantara, S., Wang, S.H., Khamkaew, C., Prapamontol, T., Janjai, S. (2018). Radiative response of biomass burning aerosols over an urban atmosphere in northern peninsular Southeast Asia. *Sci. Total Environ.* 633, 892–911. <https://doi.org/10.1016/j.scitotenv.2018.03.204>
- Penna, B., Herdies, D., Costa, S. (2018). Estimates of direct radiative forcing due to aerosols from the MERRA-2 reanalysis over the Amazon region. *Atmos. Chem. Phys.* 355–372. <https://doi.org/10.5194/acp-2018-355>
- Qi, L., Wang, S. (2019). Fossil fuel combustion and biomass burning sources of global black carbon from GEOS-Chem simulation and carbon isotope measurements. *Atmos. Chem. Phys.* 19, 11545–11557. <https://doi.org/10.5194/acp-19-11545-2019>
- Ragothaman, A., Anderson, W.A. (2017). Air quality impacts of petroleum refining and petrochemical industries. *Environments* 4, 66. <https://doi.org/10.3390/environments4030066>
- Rahim, H.A., Khan, M.F., Ibrahim, Z.F., Shoaib, A., Suradi, H., Mohyeddin, N., Samah, A.A., Yusoff, S. (2021). Coastal meteorology on the dispersion of air particles at the Bachok GAW Station. *Sci. Total Environ.* 782, 146783. <https://doi.org/10.1016/j.scitotenv.2021.146783>
- Rizza, U., Mancinelli, E., Morichetti, M., Passerini, G., Virgili, S. (2019). Aerosol optical depth of



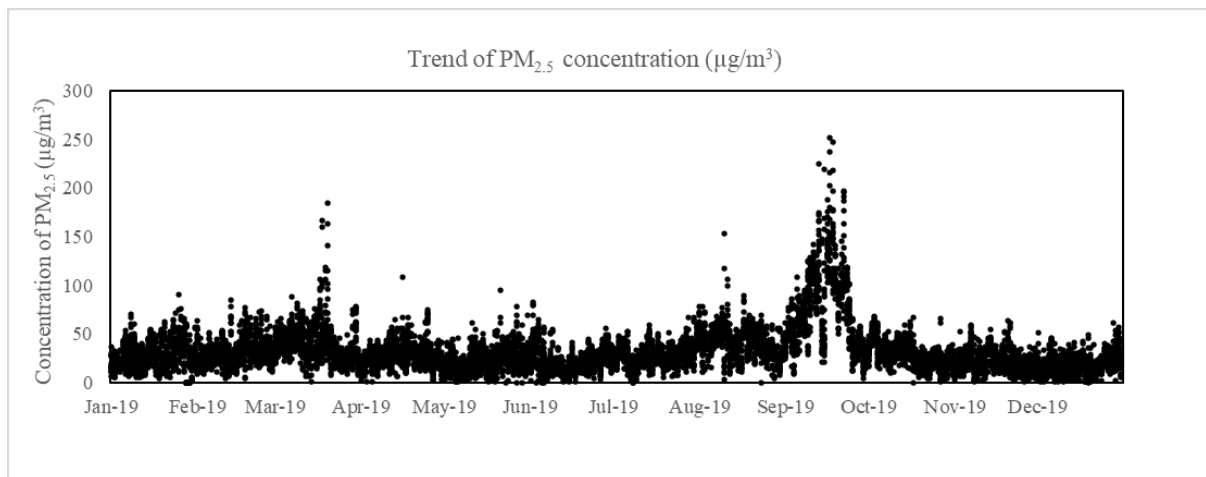
- the main aerosol species over Italian cities based on the NASA/MERRA-2 model reanalysis. *Atmosphere* 10, 709. <https://doi.org/10.3390/atmos10110709>
- Samsuddin, N.A.C., Khan, M.F., Maulud, K.N.A., Hamid, A.H., Munna, F.T., Rahim, M.A.A., Latif, M.T., Akhtaruzzaman, M. (2018). Local and transboundary factors' impacts on trace gases and aerosol during haze episode in 2015 El Niño in Malaysia. *Sci. Total Environ.* 630, 1502–1514. <https://doi.org/10.1016/j.scitotenv.2018.02.289>
- Tang, R., Huang, X., Zhou, D., Ding, A. (2020). Biomass-burning-induced surface darkening and its impact on regional meteorology in eastern China. *Atmos. Chem. Phys.* 20, 6177–6191. <https://doi.org/10.5194/acp-20-6177-2020>
- Tangang, F., Latif, M.T., Juneng, L. (2010). Climate change: Is Southeast Asia up to the challenge? The roles of climate variability and climate change on smoke haze occurrences in Southeast Asia region. LSE IDEAS, London School of Economics and Political Science, pp. 36–49.
- Tsai, Y.I., Sopajaree, K., Chotruksa, A., Wu, H.C., Kuo, S.C. (2013). Source indicators of biomass burning associated with inorganic salts and carboxylates in dry season ambient aerosol in Chiang Mai Basin, Thailand. *Atmos. Environ.* 78, 93–104. <https://doi.org/10.1016/j.atmosenv.2012.09.040>
- Vaughan, M., Garnier, A., Liu, Z., Josset, D., Hu, Y., Lee, K.P., Hunt, W., Vernier, J.P., Rodier, S., Pelon, J. (2012). Chaos, consternation and CALIPSO calibration: New strategies for calibrating the CALIOP 1064 nm Channel. Proceedings of the 26th International Laser Radar Conference (ILRC), Porto Heli, Greece, pp. 39–55.
- Wang, D., Zhou, B., Fu, Q., Zhao, Q., Zhang, Q., Chen, J., Yang, X., Duan, Y., Li, J. (2016). Intense secondary aerosol formation due to strong atmospheric photochemical reactions in summer: Observations at a rural site in eastern Yangtze River Delta of China. *Sci. Total Environ.* 571, 1454–1466. <https://doi.org/10.1016/j.scitotenv.2016.06.212>
- Watt, S., Chang, L., Jiang, N., Fuchs, D., Barthelemy, X., Scorgie, Y., Riley, M. (2017). Using HYSPLIT to forecast haze plumes during hazard reduction burns in New South Wales. CASANZ2017 Conference, pp. 1–6.
- Winker, D.M., Pelon, J., Coakley, J.A., Ackerman, Jr. S.A., Charlson, R.J., Colarco, P.R., Flamant, P., Fu, Q., Hoff, R.M., Kittaka, C., Kubar, T.L., Treut, H.L., McCormick, M.P., MéGie, G., Poole, L., Powell, K., Trepte, C., Vaughan, M.A., Wielicki B. (2010). The CALIPSO Mission. *IGARSS*, pp. 1329–1331.
- Yang, X., Zhao, C., Yang, Y., Fan, H. (2021). Long-term multi-source data analysis about the characteristics of aerosol optical properties and types over Australia. *Atmos. Chem. Phys.* 21, 3803–3825. <https://doi.org/10.5194/acp-21-3803-2021>
- Yassen, M.E., Jahi, J.M. (2007). Investigation of variations and trends in TSP concentrations in the Klang Valley Region, Malaysia. *J. Environ. Manage.* 8, 57–68. http://journalarticle.ukm.my/2247/1/2007_4_EINour.pdf
- Yin, S., Wang, X., Guo, M., Santoso, H., Guan, H. (2020). The abnormal change of air quality and air pollutants induced by the forest fire in Sumatra and Borneo in 2015. *Atmos. Res.* 243, 105027. <https://doi.org/10.1016/j.atmosres.2020.105027>
- Zainal, S., Zamre, N.M., Khan, M.F. (2021). Emission level of air pollutants during 2019 pre-haze, haze, and post-haze episodes in Kuala Lumpur and Putrajaya. *Malay. J. Chem. Eng. Tech.* 4, 137. <https://doi.org/10.24191/mjcet.v4i2.14299>
- Zhang, Y., Li, Z., Bai, K., Wei, Y., Xie, Y., Zhang, Y., Ou, Y., Cohen, J., Zhang, Y., Peng, Z., Zhang, X., Chen, C., Hong, J., Xu, H., Guang, J., Lv, Y., Li, K., Li, D. (2021). Satellite remote sensing of atmospheric particulate matter mass concentration: Advances, challenges, and perspectives. *Fund. Res.* 1, 240–258. <https://doi.org/10.1016/j.fmre.2021.04.007>

Supplementary Information:

S1: Study Period and location

The trend of PM_{2.5} Concentration ($\mu\text{g}/\text{m}^3$) in a few continuous air quality monitoring stations (CAQMS) in the west peninsular Malaysia which are located at ;

a) Sek. Keb. TTDI Jaya, Shah Alam (CA20B)



b) Sek. Men. Keb. Seri Permaisuri, Cheras (CA16W)

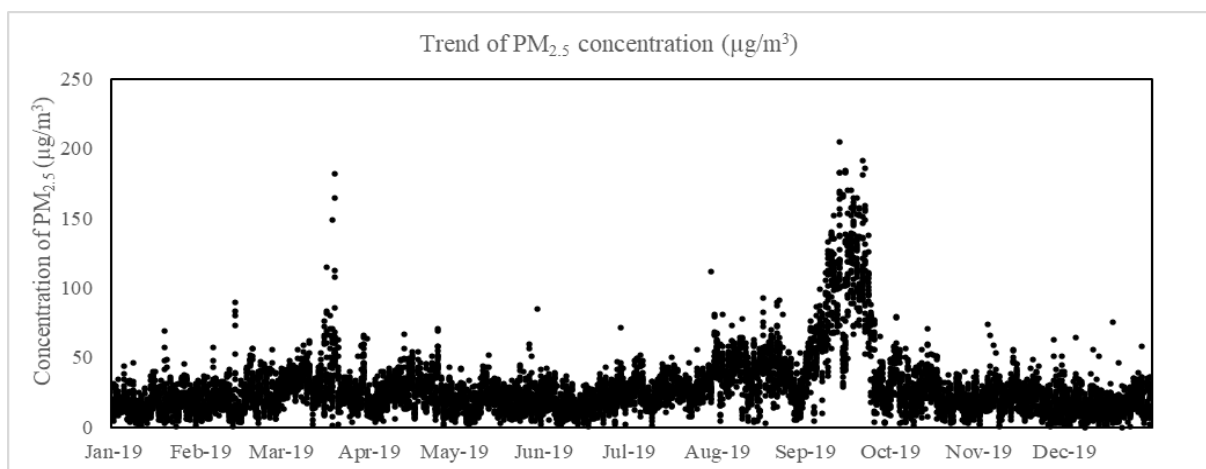


Fig. S1. Hourly trend of PM_{2.5} concentration at west Peninsular Malaysia

S2: MERRA- 2 Reanalysis Data

The PM_{2.5} concentration were obtained based on the data of aerosol subtype of BC, OC, SO₄²⁻, dust and sea salt in the MERRA-2 reanalysis. The equation that used to compute the PM_{2.5} concentration was shown in the equation 1.

$$PM_{2.5} = DUSMASS25 + OCSMASS + BCSMASS + SSSMASS25 + \text{Equation 1} \\ SO_4\text{SMASS} \cdot (132.14/96.06)$$

Where the DUSMASS25 = dust column mass concentration - PM_{2.5} (kg m⁻³), OCSMASS = organic carbon column mass concentration (kg m⁻³), BCSMASS = black carbon column mass concentration (kg m⁻³), SSSMASS25 = sea salt column mass concentration - PM_{2.5} (kg m⁻³), SO₄SMASS = SO₄ surface mass concentration (kg m⁻³) and 132.14/96.06 multiplication factor for sulfate ion.

The MERRA-2 reanalysis data were evaluated based on the performance indicator in term of error measure and accuracy measure. The mean fractional bias (MFB) and mean fraction error (MFE) were used to measure the error of the model data on predicting the PM_{2.5} concentration with the acceptable standard are within $-0.35 < x < 0.35$ and $x < 0.55$, respectively. Meanwhile, correlation coefficient was used to measure the accuracy of the model data with the acceptable standard for PM_{2.5} concentration is $x > 0.5$. The mathematical equation of error and accuracy measure were shown in equation 2 to equation 4.

$$\text{Mean fractional bias (MFB)} = \frac{1}{N} \sum_{i=1}^N \frac{M_i - O_i}{(M_i - O_i)/2} \quad \text{Equation 2}$$

$$\text{Mean fractional error (MFE)} = \frac{1}{-N} \sum_{i=1}^N \frac{|M_i - O_i|}{(M_i - O_i)/2} \quad \text{Equation 3}$$

$$\text{Correlation coefficient (R)} = \frac{1}{N - 1} \sum_{i=1}^N \left[\frac{(M_i - \bar{M})(O_i - \bar{O})}{Stdev_M Stdev_O} \right] \quad \text{Equation 4}$$

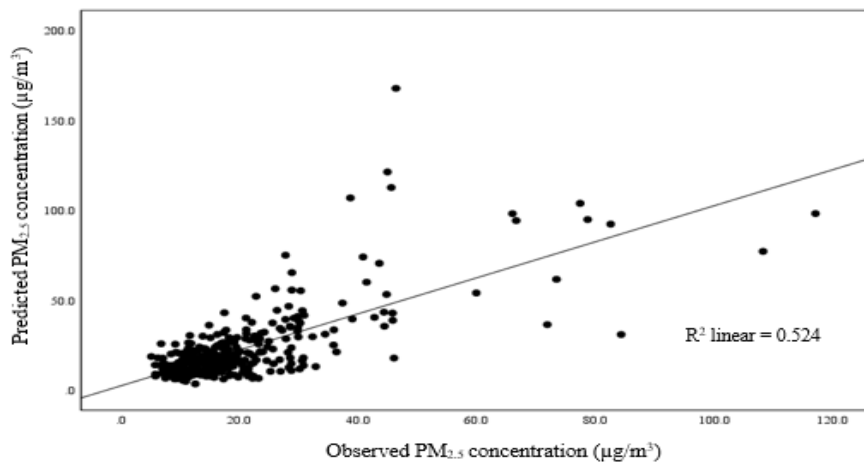
Where, the N = total number of data, M_i = the predicted values, \bar{M} = mean predicted values, O_i = the observed values, \bar{O} = mean observed values, $Stdev_M$ = standard deviation of predicted values and $Stdev_O$ = standard deviation of observed values.

The evaluation result of MERRA-2 reanalysis data on predicting the PM_{2.5} concentration at ECPM regions based on mean fractional bias (MFB), mean fraction error (MFE) and correlation coefficient (R) for three different CAQMS that involved in this study.

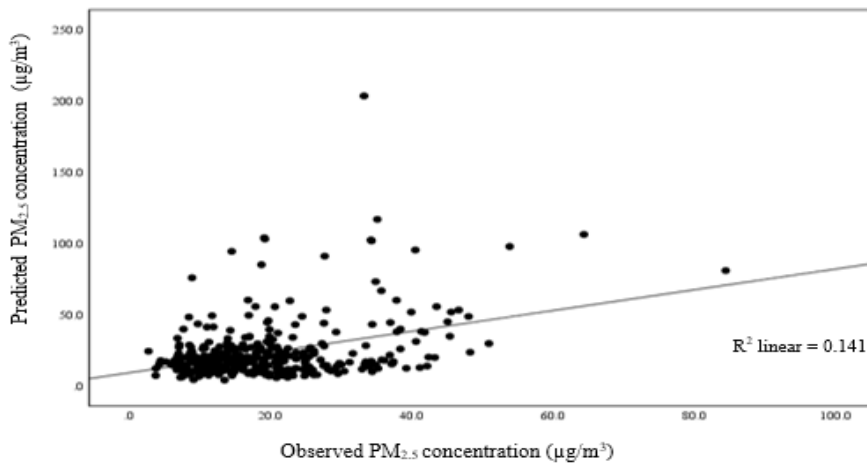
Table S1. The MERRA-2 reanalysis data evaluation result

Location	Performance Evaluation		
	MFB	MFE	R
CA42T	0.036	0.001	0.72
CA46D	0.071	0.156	0.38
CA40C	-0.028	0.001	0.50

a)



b)



c)

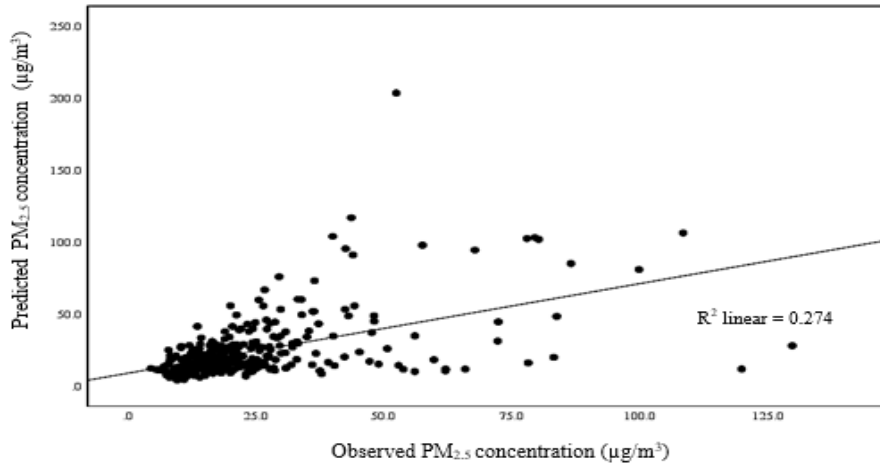
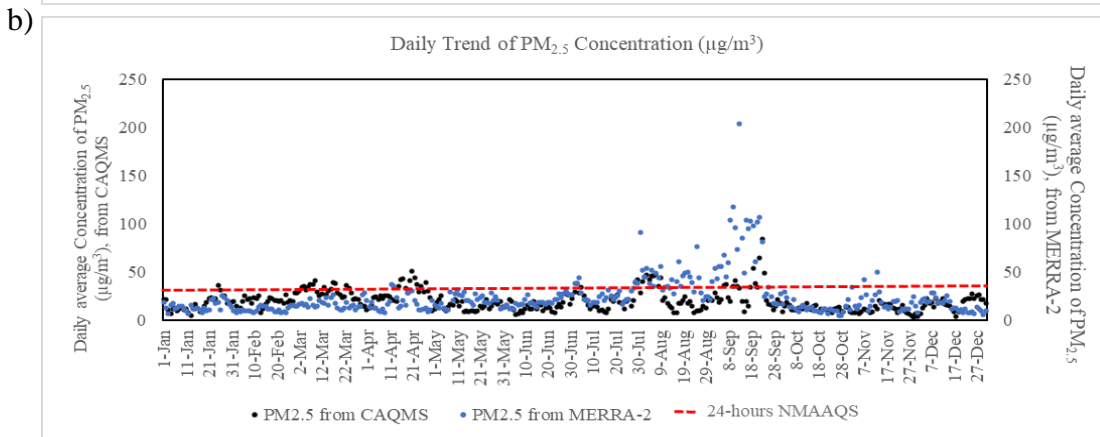
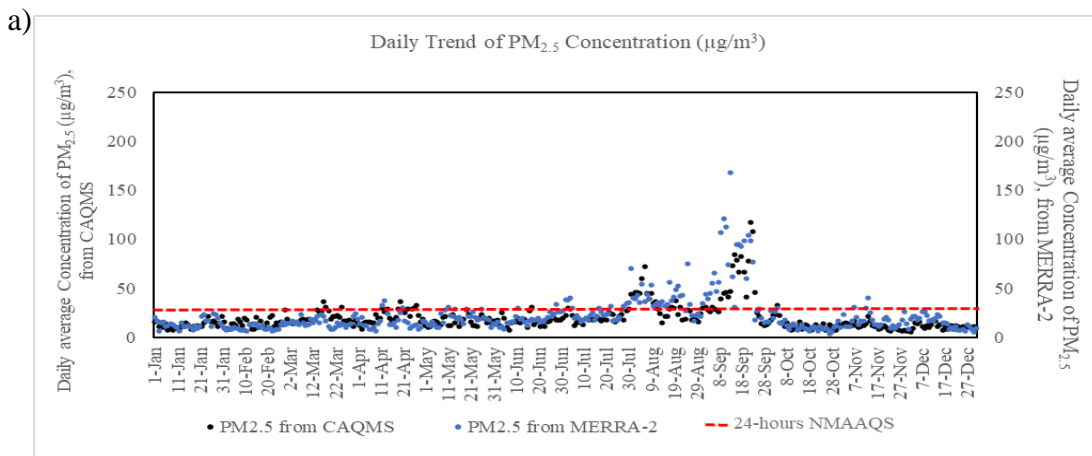


Fig. S2. Scatter plot of predicted PM_{2.5} concentration (µg/m³) against observed PM_{2.5} concentration (µg/m³) for MERRA-2 reanalysis data model at a) Terengganu, b) Kelantan and c) Pahang

Some outliers were detected for all three CAQMS especially during the peak PM_{2.5} concentration in the MERRA-2 data.



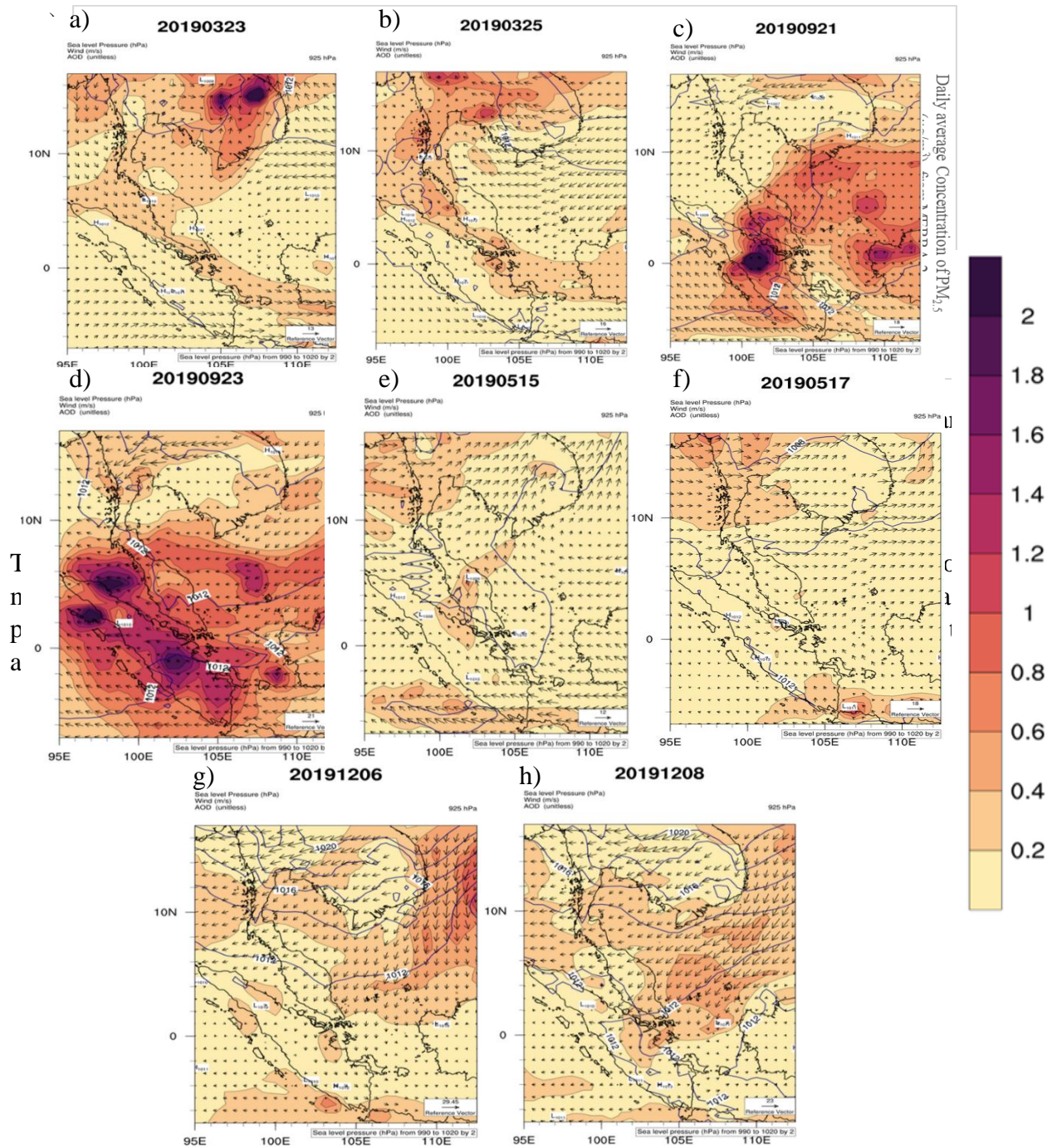


Fig. S4. The meteorological condition of wind speed, wind direction and sea level pressure during (a-b) HP1, (c-d) HP2, (e-f) LP1 and (g-h) LP2 at MC.

S3: Identification of the origin of aerosols through HYSPLIT model

HYSPLIT backward trajectories analysis has run three days continuously to trace the sources of pollutants during HP1, HP2, LP1 and LP2. The trajectories analysis for one day before and after having shown in Fig. S5 and Fig. S6.

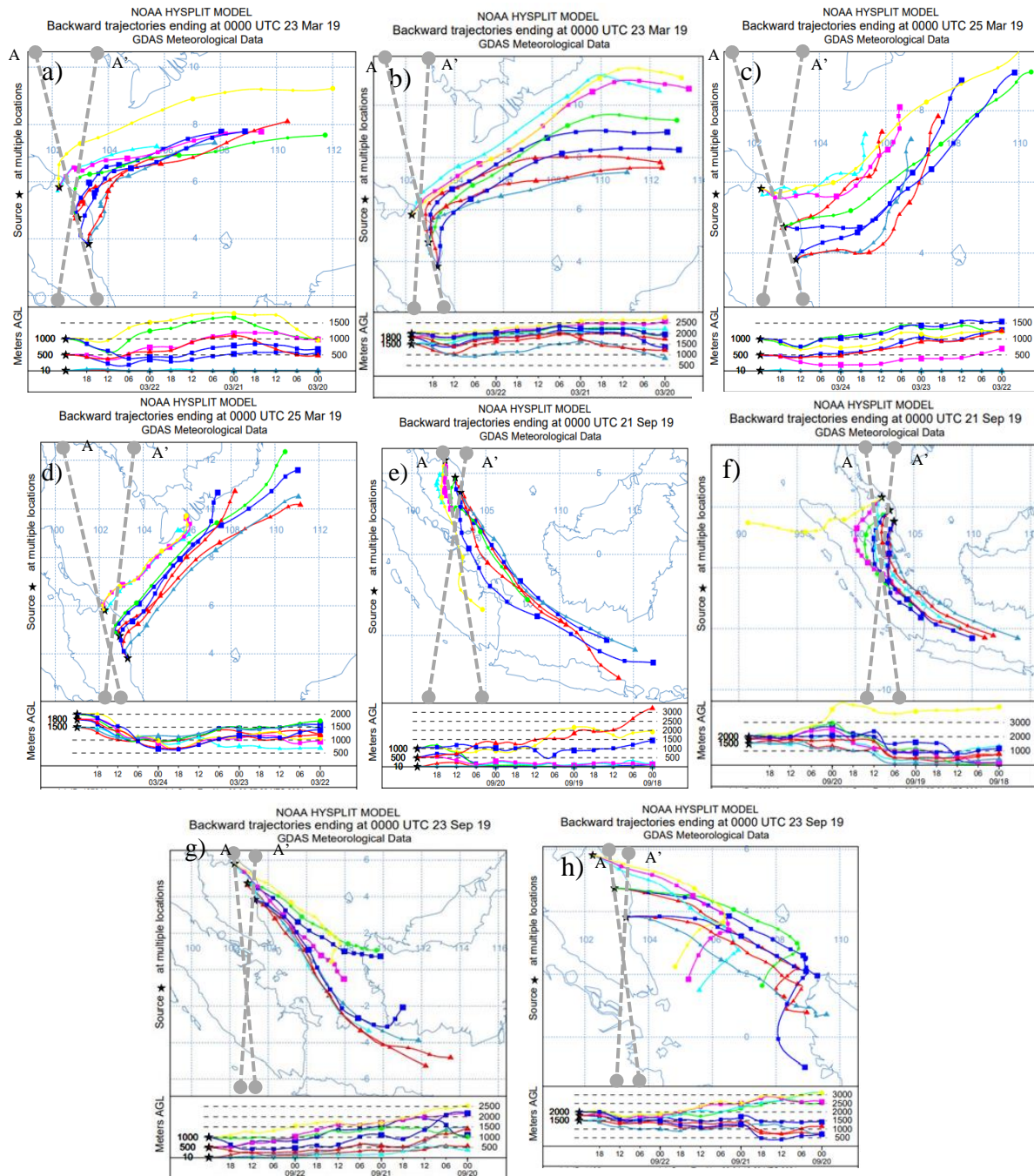


Fig. S5. Backward Trajectories Analysis at (a, c) 0-1000 m and (b, d) 1500-2000 m for HP1 while (e, g) 0-1000 m and (f, h) 1500-2000 m for HP2 on three consecutive days. Grey dotted line A (daytime) and A' (nighttime) are present as a swath of CALIOP.

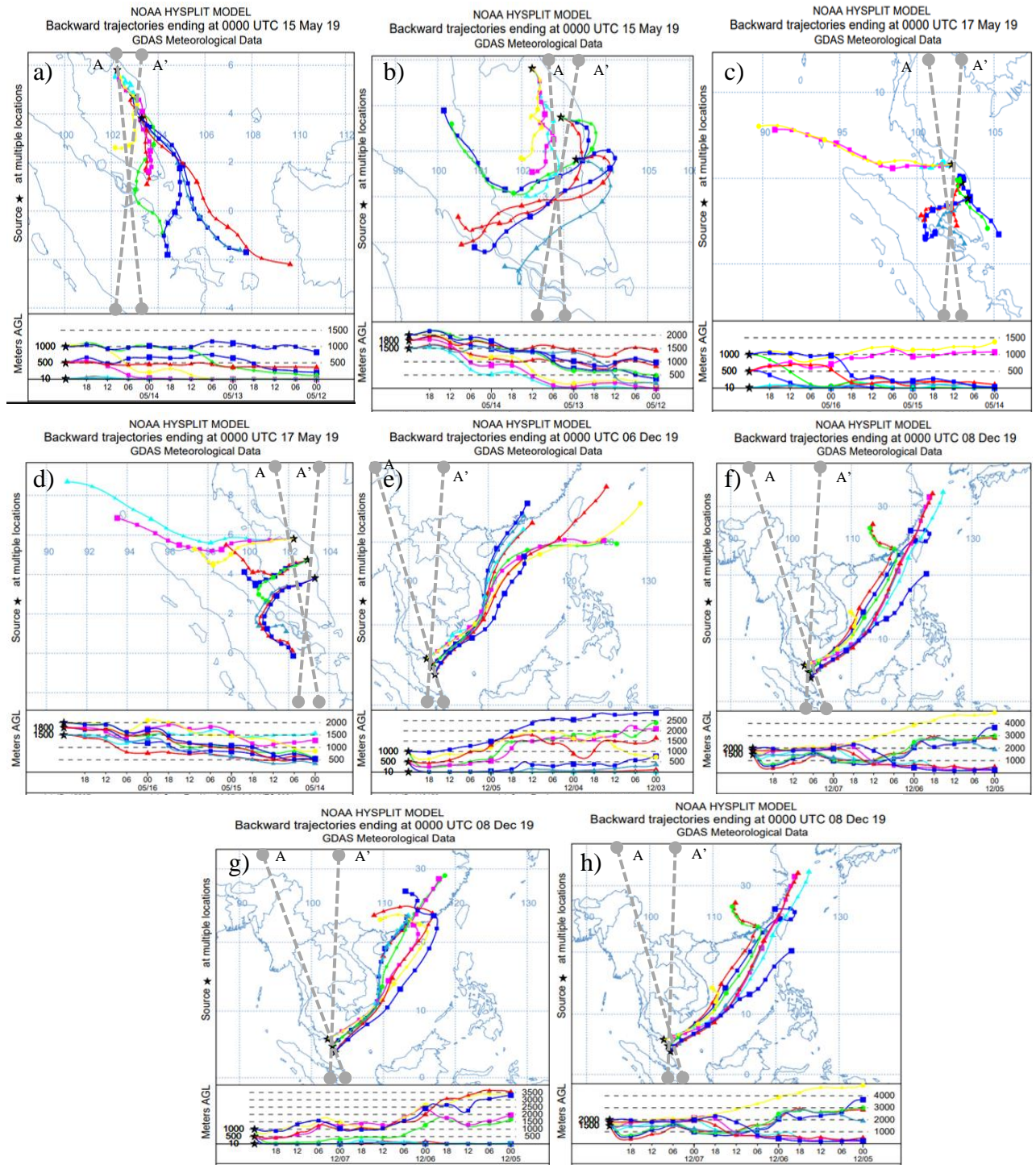


Fig. S6. Same as Fig.S5 but (a-d) for LP1 while (e-h) for LP2.